

# Fabricating and Assembling Acoustic Metamaterials and Phononic Crystals

Christabel Choi, Shubhi Bansal,\* Niko Münzenrieder, and Sriram Subramanian\*

Acoustic metamaterials (AMM) and phononic crystals (PC) have the potential to unfold a new wave of disruptive technologies to radically transform human interactions, sensory communications, and beyond. Although essential, cultivating a deep understanding of the fundamental theory and design principles is insufficient alone, in the practical advancement of AMMs and PCs. Equally important is the physical realization of these artificial structures for tangible prototyping and experimental investigation; however, such aspects are seldom discussed in literature. Herein, the fabrication and assembly approaches for AMMs and PCs are critically examined, with a tight coupling of theoretical and experimental considerations. Crucial parameters like operating frequency, materials, and geometry for efficient structural implementation are addressed. Herein, fabrication methods for specific structure types are categorized under “single-step fabrication” including printing and machining and “multi-step fabrication” like microfabrication and molding. Various “assembly” techniques are proposed, such as for ordering colloidal assemblies or fastening components without adhesives. This framework uncovers innovative designs, e.g., origami-based structures with conductive coating, only accessible if fabrication and assembly aspects form an integral part of the initial design phase. By establishing a greater understanding and awareness of these methods, a host of undiscovered pathways, opportunities, and research gaps is revealed, supporting a fresh paradigm for innovation.

## 1. Introduction

Acoustic metamaterials (AMMs) and phononic crystals (PCs) have garnered significant attention in recent years, as part of the collective driving force toward creating intelligent acoustic devices. Advancements in these fields have greatly enhanced the way we manipulate sound waves through transmission, reflection, refraction, absorption, diffraction, or attenuation. In the past decade, AMMs and PCs have enabled novel applications such as acoustic lensing,<sup>[1–3]</sup> cloaking,<sup>[4]</sup> levitation,<sup>[5]</sup> and holography.<sup>[6–8]</sup> While these exotic structures have been well explored through theoretical and numerical analysis,<sup>[9–13]</sup> their physical realization is an important topic that is rarely discussed.


Considering the ubiquity of sound and the powerful capabilities of AMMs and PCs, the impact of these acoustic structures could be phenomenal. Across the full acoustic frequency spectrum, practical applications such as noise cancellation,<sup>[14]</sup> underwater detection,<sup>[15]</sup> medical imaging,<sup>[16]</sup> and energy harvesting<sup>[17,18]</sup> could benefit

key sectors in our society like healthcare, well-being, environmental sustainability, and security. Moreover, AMMs and PCs can help to usher in next-generation technologies for personalized, immersive multisensory<sup>[19–22]</sup> experiences. The manipulation of sound can enrich the way we communicate and interact with our surroundings, not simply through audio, but also through tactile sensations. In the future, AMMs and PCs could be used in virtual reality (VR) setups,<sup>[23]</sup> compact wearable devices, and dynamic midair volumetric displays<sup>[24]</sup> that are controllable and capable of providing haptic feedback.<sup>[25]</sup> Beyond the notion that AMMs and PCs can replace phased arrays, they could readily complement one another for more precise control. In commercial devices, AMM and PC functionalities could even be combined together in different ways, e.g., transmissive and sound absorptive structures, for improved performance. To unlock the full potential of AMMs and PCs, it is therefore vital to ensure that practical, physical realization is pursued alongside theoretical investigation in the development of viable acoustic designs.

Building an AMM or PC requires some form of fabrication or assembly or both. Fabrication refers to the technologies and processes used to manufacture an object, whereas assembly refers to the strategic amalgamation of parts for a constructive purpose. AMMs and PCs can also be assembly free, i.e., the complete

C. Choi, Dr. S. Bansal, Prof. S. Subramanian  
Department of Computer Science  
Faculty of Engineering  
University College London  
London WC1E 6BT, UK  
E-mail: shubhi.bansal@ucl.ac.uk; s.subramanian@ucl.ac.uk

Prof. N. Münzenrieder  
Faculty of Science and Technology  
Free University of Bozen-Bolzano  
Bozen 39100, Italy

 The ORCID identification number(s) for the author(s) of this article can be found under <https://doi.org/10.1002/adem.202000988>.

© 2020 The Authors. Advanced Engineering Materials published by Wiley-VCH GmbH. This is an open access article under the terms of the Creative Commons Attribution License, which permits use, distribution and reproduction in any medium, provided the original work is properly cited.

The copyright line for this article was changed on 21 December 2020 after original online publication.

DOI: 10.1002/adem.202000988

structure can be directly and monolithically fabricated. More often than not, extensive design requirements can make building physical prototypes a challenging task. Desired properties, like perfect absorption or negative refraction, are mainly governed by different mechanical, geometric, and material characteristics. Hence, any discrepancies arising from imperfections in fabricated structures can negatively influence their acoustic performance. Moreover, dynamic AMM and PC designs can increase building complexity by incorporating stimuli-responsive structures and actuation mechanisms.<sup>[26,27]</sup> Prototyping multiple iterations for optimization can consume enormous time, labor, and monetary resources, which we believe can be alleviated by considering relevant physical and experimental aspects from the initial design phase.

In this Review, we critically discuss various fabrication and assembly methods to build AMMs and PCs. We first establish popular structure types that form the building blocks of AMMs and PCs and discuss how structural properties and device operation can point toward appropriate fabrication techniques. Subsequently, we classify viable fabrication techniques into the categories of “single-step” and “multi-step” fabrication. Under single-step fabrication, we first analyse 3D printing and machining technologies appropriate for AMMs and PCs operating in the audible (20–20 kHz) or ultrasonic (20 kHz–100 MHz) regimes. Then, hybrid manufacturing processes and their implications are briefly examined for more efficient structural implementation. Under multi-step fabrication, we see a range of approaches for fabricating nanoscale, heterogeneous, or soft-matter-based designs which mainly range from ultrasonic to hypersonic (>100 MHz) operating frequencies. These approaches involve microfabrication, molding and casting, and microfluidic-based wet-chemical

techniques. Thereafter, we present several assembly methods which encompass the use of adhesives, self-assembly, and fitting techniques to strategically construct AMM and PC assemblages in random or ordered arrangements. We conclude with a comprehensive outlook on further applications and future prospects. Our discussions of the relevant techniques, along with underutilized materials and research gaps, thereby provide a roadmap, promoting the development of advanced AMMs and PCs.

## 2. Types of Structures

AMMs and PCs are discussed together as they often share similar fabrication approaches and acoustic applications. Both are composed of unit cells, with each unit cell consisting of elements unique to their design. In operation, these elements interact with the impinging sound waves. The unit cells in a PC are always periodic, and the size of their elements are on an order of the operating wavelength. However, the unit cells in an AMM can be either periodic or nonperiodic, and their elements are smaller than the operating wavelength (i.e., subwavelength).<sup>[28]</sup> Planar AMMs and PCs, known as acoustic metasurfaces,<sup>[29,30]</sup> have been gaining traction in recent years. The unit cells in these 2D devices are structured in arrays, and their appealing thin, compact design offers greater versatility as compared with their bulk counterparts for wave engineering applications, especially for long wavelengths. For example, phase discontinuities can be engineered at the interface between media for targeted acoustic focusing.<sup>[8]</sup>

Traditionally, AMMs have operated through locally resonating elements,<sup>[31]</sup> as seen in colloidal suspensions (Figure 1a),<sup>[32–34]</sup> Helmholtz resonators (Figure 1b),<sup>[35–37]</sup> and membrane-type (Figure 1c),<sup>[38,39]</sup> structures. PC lattices (Figure 1d),<sup>[40,41]</sup> and

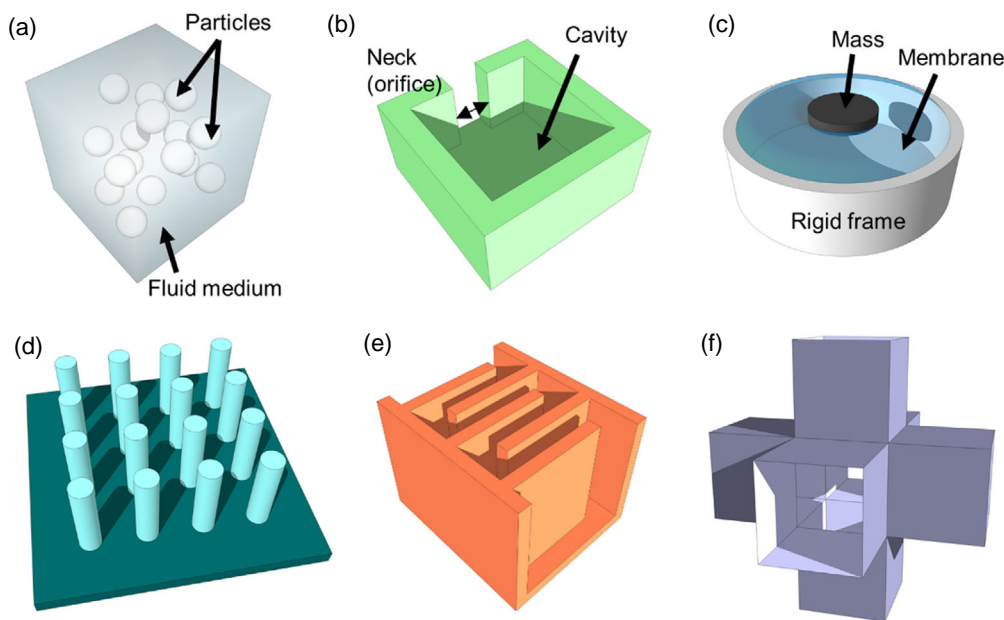


**Figure 1.** Typical AMM and PC structures. Figure 1 shows the general examples of six common structures found in AMMs and PC designs. a) Colloidal metamaterial consisting of spherical particles within a fluid medium. b) Helmholtz resonator structure with a cavity and a narrow orifice. c) Membrane-type structure with a mass at the center of the membrane, surrounded by a rigid frame. Adapted with permission.<sup>[50]</sup> Copyright 2014, Springer Nature Limited. d) Lattice structure consisting of an array of cylindrical pillars. e) Labyrinthine space-coiling structure. f) Deformable origami-based waveguide. Adapted under terms of the CC-BY license.<sup>[44]</sup> Copyright 2016, The Authors, published by AAAS.

certain AMMs,<sup>[3]</sup> rely on the mutual interaction between neighboring periodic elements within a matrix. Bandgaps that forbid acoustic transmission are formed through multiple scattering and the interference of propagating waves. Other types of AMMs may not operate through resonance but by coiling space in labyrinthine structures (Figure 1e)<sup>[42,43]</sup> or waveguiding using origami-based structures (Figure 1f).<sup>[44–46]</sup> AMM design generally revolves around the parameters of effective mass density ( $\rho$ ) and bulk modulus ( $K$ ),<sup>[31]</sup> where they can be singly negative (either  $\rho < 0$  or  $K < 0$ ) or doubly negative (both  $\rho < 0$  and  $K < 0$ ), depending on the type of structure.<sup>[47,48]</sup> While theoretically defining such parameters, we must determine the feasibility of building such structures. Numerical predictions may characterize a design for a certain scale, which may not be easily achievable experimentally. For instance, reconfigurable origami barriers for traffic noise reduction<sup>[49]</sup> were scaled down to one-seventh the original size, promoting greater experimental feasibility and efficiency in terms of power and cost.

The six common AMM and PC structures shown in Figure 1 represent very broad categories of designs. In particular, there has been growing interest in lattice-type acoustic structures that allow the topologically protected propagation of sound waves, where propagation is forbidden in the bulk but permitted on the surface. Various topological phases have been reported, such as quantum spin Hall effect topological insulators (TI),<sup>[51,52]</sup> acoustic valley Hall TIs,<sup>[53,54]</sup> and Weyl PCs.<sup>[55,56]</sup> Higher-order Wannier-type TIs<sup>[57–60]</sup> can exhibit unique boundary states in different dimensions, such as edge, corner, and hinge states. Acoustic TIs enable unusual capabilities, such as immunity to backscattering and ultra-broadband transmission.<sup>[61]</sup> Gradient refractive index (GRIN)<sup>[62–64]</sup> AMMs and PCs also tend to assume lattice configurations, and they are typically designed by spatially varying parameters such as the lattice constant or element size. The elements are nonresonant, and devices can be broadband.

Another class of AMMs is acoustic metafluids,<sup>[65–67]</sup> which have anisotropic mass densities and acoustic elastic properties resembling fluids, with extraordinary broadband capabilities. These structures provide the ability to cloak objects, which is valuable for acoustic stealth and sensing applications. Finally, for hypersonic acoustic manipulation, nanopatterned surface PCs with enhanced surface wave confinement have been developed for gigahertz wave generation and sophisticated nanoscale sensing techniques.<sup>[68–71]</sup> Besides the selected structures discussed in this Review, the covered building methods are applicable to a myriad of other reported theoretical designs in literature.

When choosing appropriate fabrication and assembly methods, it is essential to draw connections between the way they operate and the physical characteristics of the design. By assessing the specific building methods for these structures, we identify key features that define their usability and suitability. Subsequently, this knowledge can be extended toward developing and realizing other acoustic designs. For instance, labyrinthine structures impose path differences for delayed sound propagation to achieve phase or amplitude modulation. Physically, they are characterized by complex internal geometries. If they use high operating frequencies, elements are likely to be in the size range of millimeters or centimeters. To facilitate acoustic transmission or reflection, a material with a high acoustic impedance is preferred. With an understanding of available

methods, we can deduce that high-resolution 3D printing technology like polyjet printing would be a suitable choice. With polyjet printing, rigid spiraling or meandering features can be captured with high accuracy. If similar geometric complexity is found in other devices, e.g., Helmholtz resonators, the same printing technology can be applied with confidence.

Through our analysis of different structure types, we examine fabrication methods for AMMs and PCs and categorize them into “single-step” and “multi-step” techniques. Single-step fabrication can replicate elements with high precision and accuracy, compatible with structures consisting of ordered and repeating elements. Multi-step fabrication is applied for structures that are highly heterogeneous, complex, or consist of various minute features on the micro or nanoscale.

### 3. Single-Step Fabrication

In single-step fabrication, only one process (besides postprocessing) is undertaken to fabricate either a full AMM or PC or parts of it for further assembly. 3D printing and machining are the most standard techniques for this purpose, ideal for producing designs involving Helmholtz resonators,<sup>[72,73]</sup> labyrinthine structures,<sup>[42,43,74,75]</sup> and periodic lattices.<sup>[76,77]</sup> These techniques are accessible, cost effective, and simple to use. Here, rapid prototyping is possible through computer-aided design (CAD), compatible with both printing<sup>[78]</sup> and computer numerical control (CNC) machining technologies. Geometric modifications for multiple prototypes can be easily done by changing the design file, simplifying the fabrication of gradient or broadband designs with elements of varying shapes or sizes.

#### 3.1. Printing Technologies

3D printing is one of the most popular ways to fabricate AMMs and PCs because of its unparalleled manufacturing flexibility. The inherent limitations and operational style of a 3D printer can affect the type of materials, geometries, size, and resolution of the prints, including postprocessing requirements. We propose a classification of 3D-printed AMM and PC structures, into “microstructures” and “macrostructures”, to both categorize selected 3D printing technologies and emphasize their unique strengths and limitations. Direct ink writing (DIW), stereolithography (SLA), digital light processing (DLP), and polyjet printing are high-resolution technologies to support “microstructures,” whereas fused deposition modeling (FDM) and powder-bed fusion techniques are versatile and cost-effective choices for “macrostructures.” Here, “structures” refer to unit cells or elements.

AMM and PC “microstructures” are typically designed with features corresponding to wavelengths between centimeters and micrometers. AMMs and PCs have unit cells less than or equal to the wavelength of the chosen operating frequency; therefore, elements interacting with high-frequency sound waves are structurally smaller (and vice versa), i.e., ultrasonic (from 20 kHz to 10 MHz) designs would use wavelengths from 1.7 cm down to 34.3  $\mu\text{m}$ . For fabricating “microstructures,” we would generally select a high-resolution printer for a well-defined print with small physical features and a smooth surface finish to prevent unwanted sound attenuation and reflections.



Technologies like DIW allow a broad range of materials to be printed using customized inks such as graphene-aerogels,<sup>[79]</sup> liquid metal,<sup>[80]</sup> and shape-morphing liquid crystal elastomers (LCEs).<sup>[81]</sup> Dimensions of printed parts typically fall within the range of 100  $\mu\text{m}$ –10 cm, but fine deposition nozzles can have diameters of 10  $\mu\text{m}$  for higher-resolution printing. DIW technology can fabricate ultrasonic ceramic-based PCs as tight scaffolds of microscale rods (Figure 2a)<sup>[40,82]</sup> for sound damping (100–800 kHz) and acoustic focusing (2–12 MHz) applications. Here, each extruded line corresponds to the width of one rod. To date, DIW has rarely been used to fabricate AMMs, and nonceramic materials are yet to be applied to print PCs.

The benefit of high-resolution printing, like SLA (e.g., 25–100  $\mu\text{m}$ , Formlabs Form 3), is the ability to capture subtle geometric differences between elements and unit cells. A special kind of GRIN device is known as a Luneburg lens, which allows beam focusing in multiple directions.<sup>[84,85]</sup> An ideal spherical geometry would require a radially varying index profile from the center, which is challenging to fabricate as the element

size is not purely homogeneous throughout the structure. SLA technology was first used to demonstrate a 3D Luneburg lens prototype for 8 kHz,<sup>[62]</sup> whereas polyjet printing later enabled the experimental realization of a flattened design for ultrasonic (40 kHz) beam steering with an index ranging from 1 to 1.82 and a periodicity of 2 mm.<sup>[84]</sup> High-resolution SLA printing also allowed the direct fabrication of Helmholtz resonators with varying geometries in a single device for rainbow-trapping applications. A total of 40 gradient resonators with different cavity sizes were fabricated to mimic a human cochlear (Figure 2b), inducing the formation of bandgaps corresponding to different frequencies (1–10 kHz) for sound-filtering functionalities.<sup>[73]</sup> Another design used flat compact panels of asymmetric Helmholtz resonators for perfect broadband absorption (absorption coefficient,  $\alpha = 1$ ) between 300 and 1000 Hz.<sup>[86]</sup>

Vat polymerization techniques can replicate identical repeating unit cells as part of complex lattice configurations, such as third-order TIs. An anisotropic rhombohedron TI lattice was directly printed using SLA, consisting of a combination of

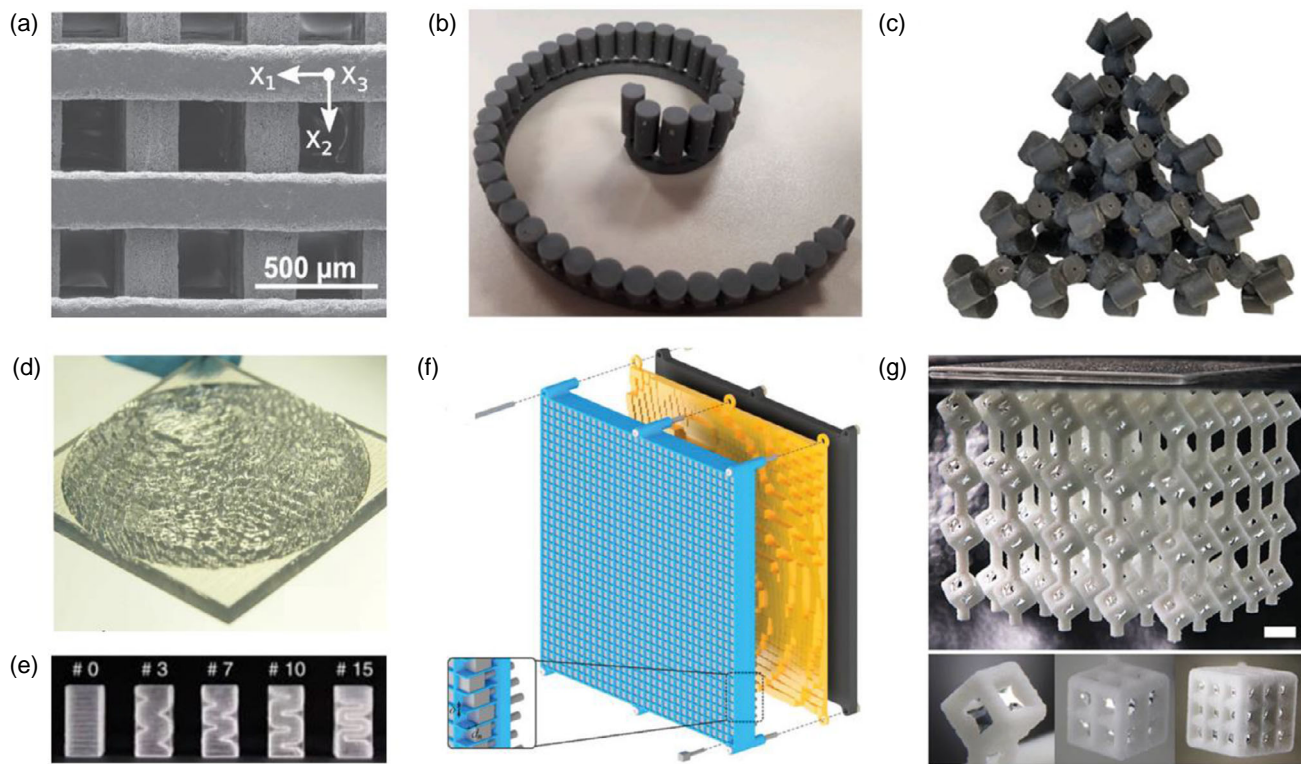


**Figure 2.** 3D-printed AMMs and PCs. a) Scanning electron microscopy (SEM) image of DIW-printed PC. Reproduced with permission.<sup>[82]</sup> Copyright 2014, AIP Publishing LLC. b) 40 SLA-printed rainbow-trapping Helmholtz resonators in a spiral, mimicking a human cochlear. Reproduced under terms of the CC-BY license.<sup>[73]</sup> Copyright 2019, The Authors, published by MDPI. c) Assembled topological pyrochlore lattice printed by DLP. Reproduced under terms of the CC-BY license.<sup>[60]</sup> Copyright 2020, The Authors, published by AAAS. d) Polyjet-printed transmission hologram using VeroClear™ material. Length of sides, 5 cm. Reproduced with permission.<sup>[6]</sup> Copyright 2016, Springer Nature Limited. e) Space-coiling metabricks. Numbers denote different coiled channel lengths corresponding to different phase shifts in units of  $\pi/8$ . Reproduced under terms of the CC-BY license.<sup>[5]</sup> Copyright 2017, The Authors, published by Springer Nature Limited. f) Reflective spatial sound modulator (SSM) metasurface. The 1024 SSM reflectors were printed by SLA, using the standard grey resin. Diameter of the cylindrical base, 1.9 mm. The frame (blue) and imprinting plate (yellow) were printed in polylactide (PLA) by FDM. High-end FDM allowed printed walls of 0.6 mm for the frame. Reproduced under terms of the CC-BY license.<sup>[8]</sup> Copyright 2020, The Authors, published by Wiley-VCH. g) Selective laser sintering (SLS)-printed hydrophobic frame for bubble formation. Scale bar, 5 mm. Below, additional pillars at the cube face to produce bubble sizes at 10, 7.5, and 5 mm, respectively (from left to right). Reproduced with permission.<sup>[83]</sup> Copyright 2019, Wiley-VCH.

coupled cylindrical resonators and connecting waveguides, where bulk corner states were observed.<sup>[59]</sup> DLP technology is similar to SLA but uses light projection instead of a laser beam to fully illuminate, rather than trace, each print slice for UV polymerization. As a result, DLP allows shorter processing times.<sup>[87]</sup> Using DLP technology, a topological pyrochlore lattice (Figure 2c) which demonstrated a third-order hierarchy of topological states was fabricated.<sup>[60]</sup> The localization of states in three separate dimensions was reported, which had implications for the stability and control of these modes.

Although both SLA and DLP are mostly limited to thermoset photopolymer materials such as epoxy resins or acrylic, adding nanoparticles to the resin can modify properties such as mechanical strength or electrical conductivity. It has also been proposed that SLA could substitute complicated microfabrication and molding techniques such as soft lithography, demonstrated through printable polydimethylsiloxane (PDMS, Sylgard-184) microdevices.<sup>[88]</sup> While out-of-plane thicknesses are limited for soft lithography processes, 3D printing can fabricate soft and deformable 3D architectures, potentially allowing the incorporation of microfluidic channels or pneumatic systems. Here, inspiration can be drawn from the field of soft robotics, where DLP-printed elastomers have been effectively used for pneumatically controlled grippers and actuators.<sup>[89]</sup> An integrated and fully automated setup is also possible, showcased in an entirely microfluidic-based soft robot, fabricated via a combination of embedded printing and soft lithography.<sup>[90]</sup> Using similar design principles, DIW could instead be used in tandem with SLA and adapted for the integrated actuation of AMM and PC devices.

It is noteworthy that a major drawback of vat polymerization techniques is the inability of continuous multimaterial printing. Moreover, standard clear resins for SLA require postprocessing for optical transparency, and incomplete or improper curing of the resin may alter print geometry (e.g., bending), affecting the performance of AMM or PC. Polyjet<sup>[62,91]</sup> printing presents itself as an attractive alternative, with its ability to directly print multimaterial composite structures using photopolymers, exhibiting an extremely smooth surface finish. Surface roughness for a glossy finish can go as low as 0.5  $\mu\text{m}$  (root mean square, RMS). Unfortunately, polyjet printing also suffers from certain limitations. The photosensitivity of materials may cause them to become brittle and degrade in UV light over time. Water-soluble support material used for overhangs (e.g., SUP706) may also be challenging to remove in narrow cavities or channels, even with water jetting.

Nevertheless, polyjet or multijet printing can easily produce highly transparent prints (Figure 2d)<sup>[5,6]</sup> using standard materials such as Stratasys' acrylate-based VeroClear™. Optical transparency is beneficial for structures with intricate internal geometries, as it provides additional visibility and imaging capabilities. This is especially useful for reconfigurable designs which rely on variable physical states, permutations, or combinations, of the involved elements and unit cells. For example, Figure 2e shows 5 out of 16 space-coiling metabricks which can be strategically assembled into a metasurface for any desired diffraction-limited spatial sound profile.<sup>[5]</sup> Every brick is different, and their optical transparency allows them to be visibly distinguished. Rather than assembling unit cells, another design consisted of

a fixed array of transparent Helmholtz resonators that derived their tunability from precisely controlling the water level within each cavity.<sup>[92]</sup> Changing the volume of the cavities allowed phase and amplitude modulation. For future research, optical transparency could play a central role in the development of optoacoustic AMMs, where the manipulation of both visible light and sound could be optimized in a combined fashion.

Low-frequency structures are mostly designed for the audible regime from 20 Hz to 20 kHz, and elements are in the range of millimeters to centimeters. Very-high-resolution printers are not necessary for “macrostructures,” which make FDM an obvious choice to print low-frequency AMMs and PCs.<sup>[72,74]</sup> Newer models can even produce layer thicknesses down to  $\approx 0.1$  mm. FDM printers are generally affordable and simple to operate, making them popular for both industry and consumer use. They mainly produce hard prints through the use of thermoplastic filaments, which are useful for physical boundaries with high acoustic impedances to facilitate the reflection or transmission of airborne acoustic waves. The three most common and accessible materials used for AMMs and PCs are acrylonitrile butadiene styrene (ABS),<sup>[93,94]</sup> polylactide (PLA),<sup>[8,95,96]</sup> and polycarbonate.<sup>[97,98]</sup>

Due to layer-by-layer extrusion, FDM prints are often characterized by a rough layered texture. Postprocessing can significantly improve surface finish, using methods such as chemical vapor treatment, ultrasonic surface rolling, or polishing.<sup>[99,100]</sup> For example, an ABS sample with a 0.1 mm-layer height from the printed wall was polished down using acetone vapor to an improved surface roughness of 0.8  $\mu\text{m}$ .<sup>[101]</sup>

“Macrostructures” can also be fabricated via inexpensive powder-bed fusion techniques such as SLS and selective laser melting (SLM).<sup>[102–105]</sup> Recently, broadband acoustic transmission at the water-to-air interface was demonstrated by SLS-printed Nylon (FS3300PA) structures (Figure 2g).<sup>[83]</sup> The metasurface allowed almost-perfect underwater transmission at resonance, by creating architected bubble formations using the intrinsically hydrophobic-printed frame. Despite the metasurface exhibiting numerous overhangs, powder-bed fusion prints can remain highly stable during printing without needing support material, and waste powder can also be reused. This example reflected a smart coupling of theoretical design and sensible fabrication and material choices. Besides Nylon, other powdered raw materials including metals such as aluminum alloys, stainless steel, and titanium can also be obtained.<sup>[106,107]</sup> Printing entire geometries with metal eliminates unnecessary secondary processes such as welding, especially for complex features.

A reconfigurable ultrasonic (40 kHz) reflective AMM was recently reported, consisting of both “microstructures” and “macrostructures” (Figure 2f).<sup>[8]</sup> The planar metasurface could enable acoustic focusing as well as multiplane holography. It consisted of small reflector elements (cylindrical base, 1.9 mm) that were fabricated by SLA and polyjet printing (for  $16 \times 16$  array), whereas the larger imprinting plates were FDM printed using PLA. These imprinting plates are encoded with the desired collective phase response, subsequently positioning the reflectors at different heights to induce specific phase delays. Here, we see how different printing technologies can complement one another to optimally fabricate different geometric elements.

### 3.2. Machining

Subtractive manufacturing has been around for centuries, and many involved processes are still relevant today, even for metamaterials and PCs. Machining is a negative, i.e., subtractive process, whereby the resulting object is sculpted from the initial work piece, such as a piece of acrylic or slab of metal. In comparison with 3D printing, there is greater control over the properties of the raw material being machined, such as mechanical strength and hardness. Machining can also deal with high-volume or heavy-duty parts at a lower cost. Like conventional 3D printing, the covered machining processes are mainly useful for operating frequencies within the audible (20 Hz–20 kHz) and ultrasonic (>20 kHz) regimes.

Milling and drilling are popular multipoint mechanical machining processes that can either be automatic or be manual, typically using cylindrical rotating cutting heads. Minimum feature size is dependent on the size of the tool head. These technologies have been used to fabricate AMMs, exhibiting hyperbolic dispersion, often characterized by arrays of perforations or grooves, such

as hyperlenses for imaging applications (Figure 3a).<sup>[108–110]</sup> Cavities can also be cut into different materials, seen in an AMM with a drilled array of ultrasonic aluminum Helmholtz resonators,<sup>[35]</sup> and a valley topological PCs with milled acrylic channel-cavity unit cells.<sup>[111]</sup>  $1 \times 1$  mm cylindrical necks of Helmholtz resonators demonstrated how features can be easily machined to high accuracy and precision. Although CNC mills are good at making perforations and surface contours, they generally have trouble with internal corners. Hence, unlike 3D printing, 3D structures composed of machined parts often require a secondary assembly step. However, milling can produce structures with an exceptionally high-quality surface finish. A milled surface can exhibit a surface roughness as low as  $0.2 \mu\text{m}$ .

Water jet machining (WJM) is a mechanical machining process that cuts samples using pressurized water between 200 and 400 MPa. Both 2D and 3D structures can be machined, from materials like glass, wood, or metal, with thicknesses up to  $\approx 230$  mm. However, before using WJM, it is important to ensure that the AMM or PC material is corrosion resistant. WJM can precisely cut soft materials into repeating patterns, as

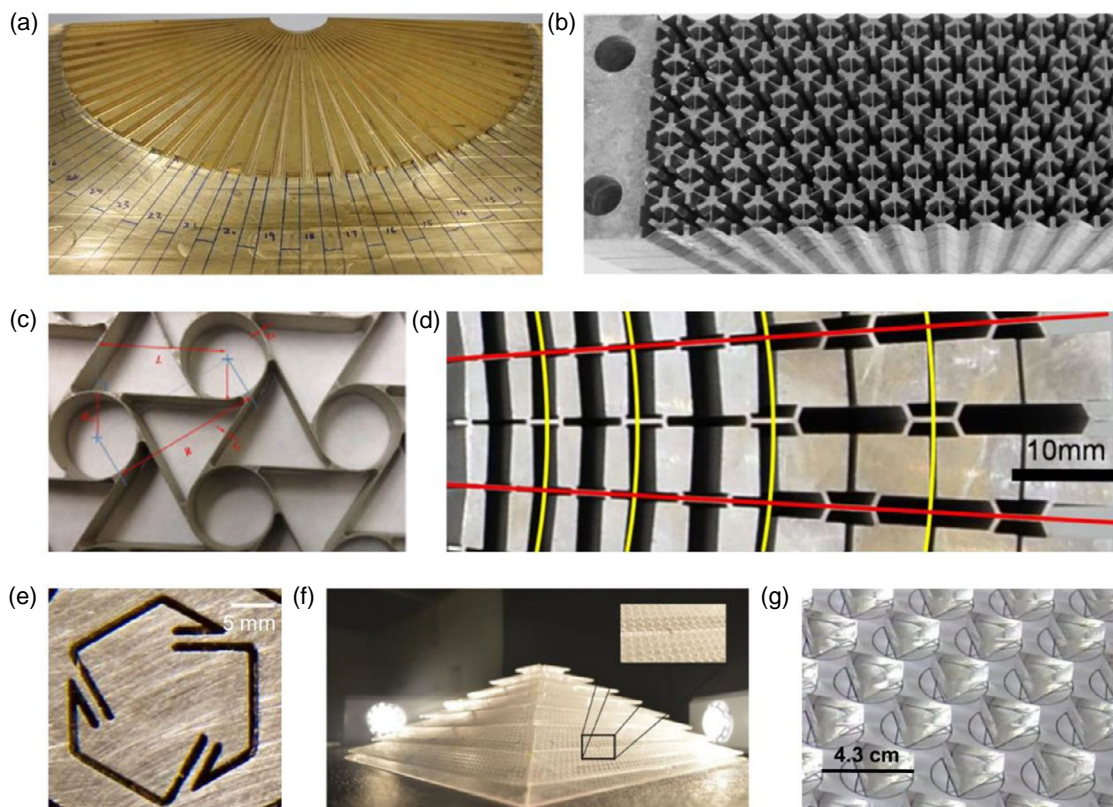


**Figure 3.** Machined structures. AMM and PC structures fabricated via mechanical and thermal machining processes. a) Acoustic magnifying hyperlens with 36 brass fins fabricated by CNC milling. Fins have a radius from 2.7 to 21.8 cm. Reproduced with permission.<sup>[110]</sup> Copyright 2009, Springer Nature Limited. b) Foam-like metallic PC lattice fabricated by WJM. The widths of interconnections are 0.5 mm and the sides of a regular hexagon are 6.445 mm. Reproduced with permission.<sup>[112]</sup> Copyright 2013, AIP Publishing LLC. c) Aluminum chiral metamaterial beam fabricated by WJM. Each circular inclusion has a diameter of 15 mm, and wall thicknesses are at 0.5 mm. The vertical thickness is 25.4 mm. Reproduced with permission.<sup>[113]</sup> Copyright 2014, Elsevier B.V. d) Aluminum broadband acoustic cloak fabricated by electrical discharge machining (EDM). Reproduced with permission.<sup>[114]</sup> Copyright 2017, American Physical Society. e) Stainless steel chiral microstructure. Scale bar, 2 mm. Reproduced with permission.<sup>[77]</sup> Copyright 2014, Nature Springer Limited. f) An omnidirectional acoustic cloak. The sides of the square base have an approximate length of 34.3 cm, whereas the vertical height can extend from 5.7 to 11.4 cm. Reproduced with permission.<sup>[4]</sup> Copyright 2014, Nature Springer Limited. g) Acrylic prisms cut to build a sonic crystal. Reproduced with permission.<sup>[53]</sup> Copyright 2017, Springer Nature Limited. e–g) are structures fabricated by the direct laser-cutting technique.



demonstrated by an elastomeric chiral lattice,<sup>[115]</sup> similar in design to an aluminum lattice beam for broadband vibration attenuation (Figure 3c).<sup>[113]</sup> Figure 3b shows a foam-like metallic PC<sup>[112]</sup> built for acoustic focusing, consisting of 15 5 mm-thick plates cut by WJM. Each slab was machined with intricate honeycomb lattices and later stacked and glued. This simple method of assembly is further covered in a later section (Section 5).

EDM is an unconventional thermal machining process that removes hard metals through electric sparks within a dielectric medium. Unlike CNC mills, EDM can better machine sharp internal corners and high-aspect-ratio features with a minimum feature size of  $\approx 0.25$  mm, highly beneficial for AMMs with deep, narrow inclusions or thin walls. EDM mostly machines conductive materials. High-precision EDM has been utilized to fabricate metafluids,<sup>[66]</sup> which can exploit negative refraction using prisms<sup>[65]</sup> and support underwater cloaking. The acoustic cloak<sup>[114]</sup> in Figure 3d was made from a block of aluminum, consisting of five layers of unit cells with the smallest rib thickness of 0.35 mm. The cloak had a height of 50 mm and exhibited broadband performance in frequencies of 9–15 kHz. Other examples include planar AMMs and PCs for lensing and wavefront manipulation, such as a holey GRIN PC and a hexagonal aluminum matrix for generating underwater plane waves from cylindrical waves within the range of 15–23 kHz.<sup>[64,116]</sup>

Another thermal machining process is direct laser cutting, popular for fabricating origami- and kirigami-based mechanical metamaterials.<sup>[117,118]</sup> Similar techniques are used to fabricate foldable and tunable AMM designs,<sup>[44]</sup> where quality and cut-rate rely on the power, material thickness, and type of laser. Unlike WJM, structures are typically 2D, and material thicknesses cannot exceed  $\approx 25$  mm. In particular, conventional CO<sub>2</sub> lasers mostly cut nonmetal material thicknesses  $< 12$  mm.

Direct laser cutting is a highly flexible technique that can cut out both patterns and separate components. Sophisticated shapes were outlined on sheets of metal (Figure 3e)<sup>[77]</sup> and polymer membranes (10–300  $\mu\text{m}$  thick)<sup>[119]</sup> for lensing and imaging applications. Other than intricate shapes, numerous laser-induced circular holes that were perforated into acrylic sheets have been used to construct an omnidirectional acoustic cloak for airborne sound (Figure 3f).<sup>[4]</sup> Another interesting application is the sculpting of different side surfaces of a Weyl PC lattice with woodpile configuration.<sup>[120]</sup> The geometric surface terminations were laser cut, enabling surface acoustic waves (SAW) to be either positively or negatively refracted at different interfaces. Moreover, besides directly patterning AMMs and PCs, a high volume of identical parts can be machined. A TI was assembled from hundreds of laser-cut acrylic prisms, which behaved as rotating anisotropic scatterers (Figure 3g).<sup>[53]</sup> Not only were acoustic valley Hall edge modes observed, the tunable TI possessed internal degrees of freedom as the scatterers modulated frequency bandgaps.

In the cases where both machining and printing can fabricate a certain structure, we can evaluate the trade-offs to choose between them, depending on the application and available resources. For example, printing a complex metallic structure via SLM would result in diminished overall surface quality. Conversely, machining such a complex structure could necessitate a further assembly step which requires more time and monetary resources.

### 3.3. Hybrid Manufacturing

Hybrid manufacturing leverages the strengths of different single-step processes via integrated fabrication approaches. Additive–subtractive processes can reduce time and cost, improve tolerances, and increase surface quality, particularly for metal parts. Recently a novel six-axis hybrid setup was reported,<sup>[121]</sup> using a robotic arm compatible with changeable printing and machining heads and a heated print bed. The integrated setup allowed multiplane processing with minimal material wastage. Moreover, multiaxis printing and machining with more degrees of freedom could reduce the need for support structures, lessening the burden of postprocessing. Subtractive–subtractive hybrid micromachining systems have combined micro-EDM ( $\mu\text{-EDM}$ ) with micro-electrochemical machining ( $\mu\text{-ECM}$ ) for shaping and finishing microscale cavities.<sup>[122]</sup> Such micromachining processes could both rival or complement complicated microfabrication techniques. Hybrid manufacturing can maximize the quality and production of AMMs and PCs, also encouraging the future integration of microelectromechanical systems (MEMS) for miniaturization and dynamic high-frequency operation in the megahertz range and beyond.

## 4. Multi-Step Fabrication

Single-step techniques are insufficient to fabricate all kinds of AMMs and PCs. In the instances where the structures are highly heterogeneous or consist of various minute features on the micro or nanoscale, we require multiple processes, besides printing and machining.

### 4.1. Microfabrication

Traditionally used in the semiconductor industry, microfabrication can fabricate micro or nanoscale structures not easily accessible via other technologies. Here, the maximum size of in-plane structures is restricted by the substrate's planar dimensions, whereas out-of-plane structures are typically limited to thicknesses  $< 500$   $\mu\text{m}$ . Microfabrication involves multiple processes, like deposition and lithography. This technique has fabricated high-frequency (ultrasonic and hypersonic regime) AMMs, and mainly PCs,<sup>[123]</sup> for specific applications such as SAW manipulation,<sup>[124]</sup> often used in microfluidic applications like sensing. SAW-based devices typically use acoustic frequencies ranging from 5 to 159 MHz, sometimes going higher into the gigahertz range.

In microfabrication, nanometer layers can be easily deposited onto substrates, which is not possible using conventional high-resolution 3D printers such as SLA and polyjet printing. Using thin-film deposition, compact, heterogeneous metasurfaces could be engineered with high surface quality and low tolerances. Depending on substrate quality, an RMS roughness in the nanometer range is assuredly achievable. Surface modifications of material layers can be used to exhibit advanced properties such as enhanced adhesion, hydrophobicity, and conductivity.

We also see dry plasma-etching processes like reactive ion etching (RIE) and deep reactive ion etching (DRIE) being used for AMM and PC fabrication.<sup>[36,63]</sup> These processes can be

isotropic or anisotropic, producing very little undercut, helpful for making high-aspect-ratio features. For example, a large array of Helmholtz resonators was etched into a 1 mm-thick silicon wafer using DRIE, with each neck width at 50  $\mu\text{m}$ .<sup>[36]</sup> This 2D inertial AMM was developed for sound attenuation (up to 18 dB), in the ultrasonic regime. A vapor release etch that provides isotropic etching using xenon difluoride ( $\text{XeF}_2$ ) can also be used to release fabricated structures from substrates like polysilicon.<sup>[125]</sup> In a recent article, a molecular etching technique was used to etch through 2 mm of steel to fabricate a metalens that could produce super-oscillation wave packets, demonstrating acoustic tweezing and acoustic imaging. The lens, shown in **Figure 4a**, used an operating frequency of 1 MHz.<sup>[2]</sup>

A combination of wet and dry etching techniques was utilized to etch graduated apertures through an entire 80  $\mu\text{m}$ -thick quartz substrate, to produce a GRIN PC lens for Lamb wave focusing and wave guiding (Figure 4c).<sup>[63]</sup> GRIN elements are ordered with varying periodicities, which might seem challenging to fabricate on a micronscale. However, in microfabrication,

lithography masks can easily transfer the entire pattern, enabling the parallel fabrication of all elements at the same time, as opposed to previously discussed single-step serial processing techniques. By incorporating microfabrication processes alongside printing or machining GRIN lenses, the minimum perforation size of the index profile could be reduced, potentially enhancing their performance.

Microfabrication patterning processes come in many forms including conventional photolithography, soft lithography, two-photon lithography, electron-beam lithography (EBL), and focused ion-beam (FIB) structuring. Soft lithography is a type of micromolding and embossing technique often used for microfluidic device fabrication. The entire process may involve EBL to pattern the mold.<sup>[127]</sup> Soft lithography is highly compatible with elastomeric materials like polydimethylsiloxane (PDMS), which was seen in the realization of a bubble PC.<sup>[128]</sup> The PC consisted of periodic air cavities embedded within soft matrix layers that could be stacked. It was found that hybridization bandgaps relied on the lattice constant and size of cavities, whereas the Bragg gap

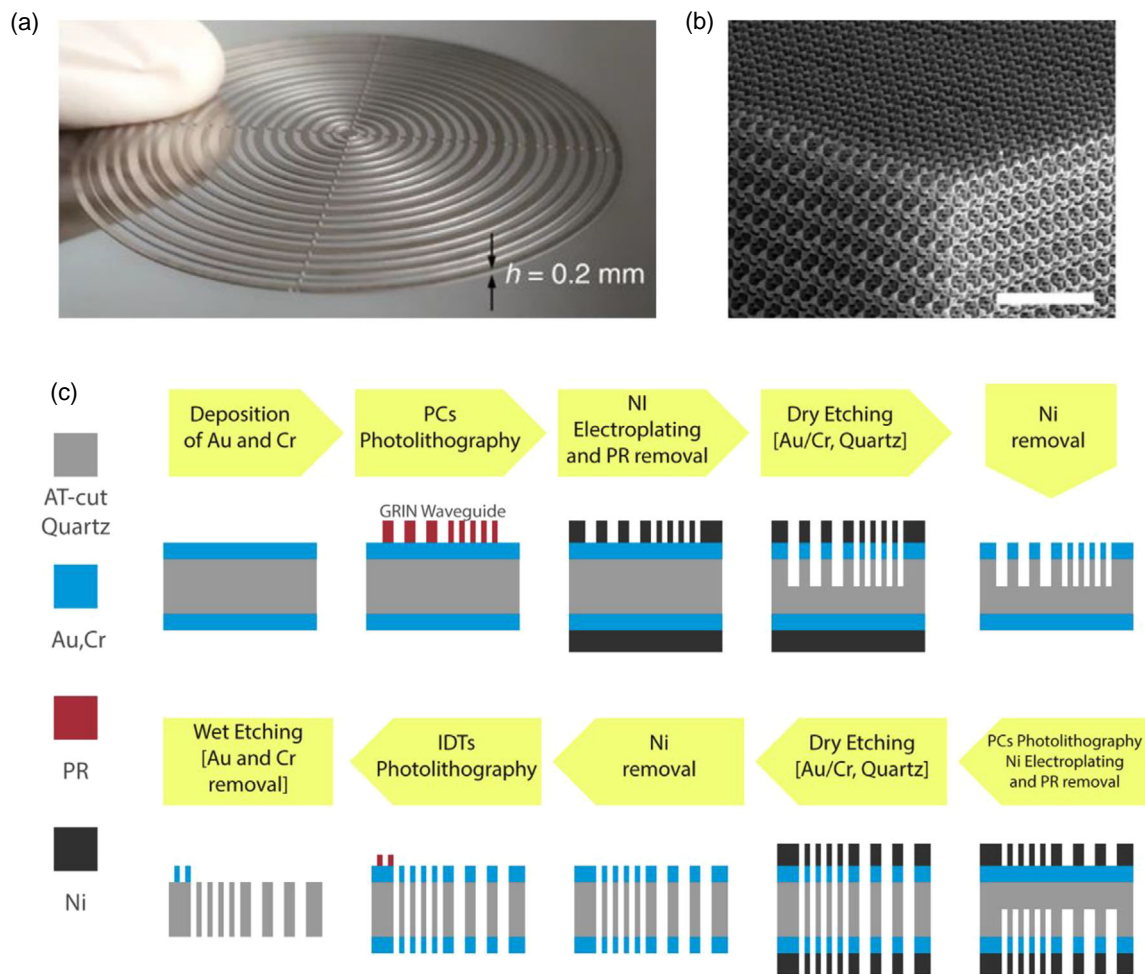


**Figure 4.** Structures fabricated using microfabrication methods. a) Ultrasonic metalens, having a thickness  $\approx 0.13\pi$  of the operating frequency. Reproduced under terms of the CC-BY license.<sup>[2]</sup> Copyright 2019, The Authors, published by Springer Nature Limited. b) SEM image of an AMM (with tapered truss elements) fabricated by two-photon lithography. Scale bar, 200  $\mu\text{m}$ . Reproduced with permission.<sup>[126]</sup> Copyright 2016, American Physical Society. c) Fabrication process flow for GRIN PC lens. “PR” refers to photoresist, and “IDT” refers to interdigital transducers. “Au,” “Cr,” and “Ni” are the chemical symbols for gold, chromium, and nickel, respectively. Adapted with permission.<sup>[63]</sup> Copyright 2014, Elsevier B.V.



depended on the distance between layers. Two-photon lithography is a special method that exposes the PR in volume elements using a controlled laser to pattern 3D nanoscale structures. Figure 4b shows an ultrasonic microlattice fabricated using this technique, that operates through the formation of hybridization bandgaps.<sup>[126]</sup>

With the emergence of surface PCs operating in the hypersonic regime from 1 to 100 GHz, powerful techniques such as EBL<sup>[129]</sup> are required for precise nanopatterning down to a few nanometers. EBL is entirely maskless as it utilizes a focused beam of electrons to scan and pattern a resist layer on the substrate, allowing greater flexibility in processing complex features and designs. This method was utilized to fabricate an array of pillars (top diameter, 170 nm) in a surface PC for frequencies within 2–7 GHz.<sup>[70]</sup> To directly structure the substrate, FIB technology can not only pattern, but also micromachine via local etching or milling. Micro or nanoscale structures can also be grown using this technique.<sup>[130,131]</sup> FIB is promising for hypersonic PC fabrication, demonstrated for a 2D freestanding silicon membrane operating at a frequency of 33 GHz.<sup>[132]</sup> However, such particle-based processes are currently better suited for low-volume production due to high production costs and slow processing times.

In recent years, surface PCs have also played a major role in advanced nanometrology research for reliable characterization, mass-sensing applications, and nondestructive testing of nano-systems.<sup>[133–135]</sup> Schemes involving the optoacoustic excitation of surface PCs offer unprecedented sensitivity for detecting even picometer-range displacements, using technologies such as extreme ultraviolet (EUV) tabletop laser sources.<sup>[71]</sup>

Apart from being able to fabricate complex AMM and PC designs, microfabrication can provide the means for active control and tunability. Integrated thin-film circuits can be patterned on flexible<sup>[136]</sup> or rigid substrates for electronic or electromagnetic actuation capabilities, thereby creating opportunities for dynamically reconfigurable acoustic devices. Although printing technologies like DIW can fabricate circuits, high-quality insulators are generally difficult to print. Further miniaturization of high-frequency AMM and PC designs via microfabrication approaches can pave the way for future integration into commercial devices, which have not yet been attempted.

## 4.2. Molding and Casting

Molding and casting is a viable method to fabricate soft and deformable structures for AMMs and PCs. It is usually a two-step process, where the mold is initially fabricated, prior to the casting and curing of the desired material. The mold may be fabricated using the previously discussed technologies such as 3D printing. Only certain materials are suitable for casting, such as resin, or silicone, which can conform into any shape and cure into a rubber-like solid. This method is advantageous, whereby elastomers or mixtures with altered properties (e.g., magnetic, conductive) can be molded into functional shapes and even be actuated for actively tunable AMMs and PCs. For instance, Fe<sub>3</sub>O<sub>4</sub> particles were embedded into a silicone mixture using a two-roll mill, to cast a membrane that was actively responsive to magnetic fields.<sup>[38]</sup> Another magnetically tunable AMM (Figure 5a)<sup>[48]</sup> was cast into the hollow channels of a water-soluble sacrificial

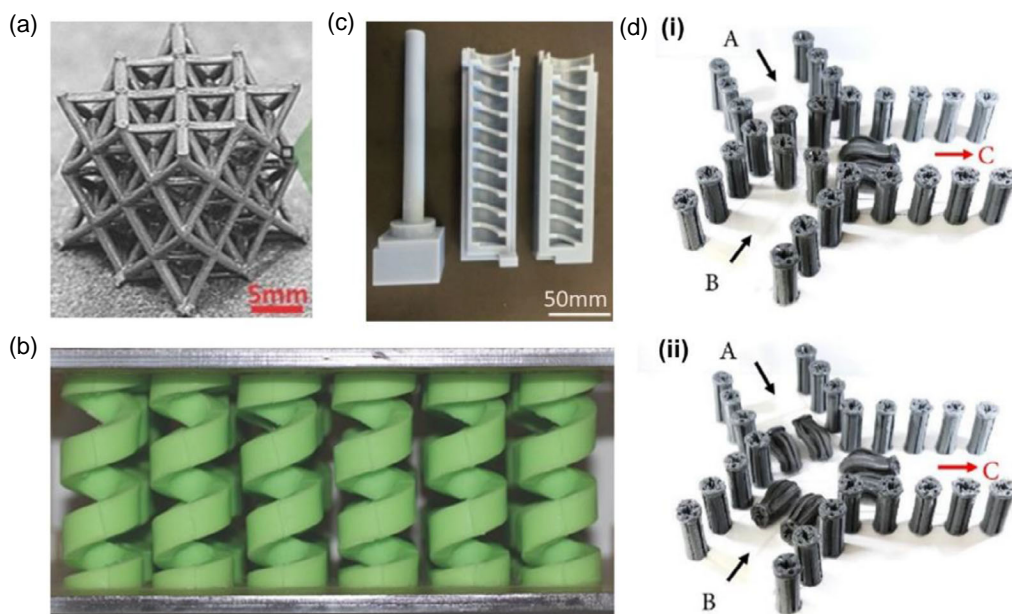


**Figure 5.** Different structures fabricated via molding and casting techniques. a) Magnetoactive AMM cast from the water-soluble mold, fabricated by projection of micro-SLA. Reproduced with permission.<sup>[48]</sup> Copyright 2018, Wiley-VCH. b) Undeformed vinylpolysiloxane elastomeric helices for controlled acoustic switching. When deformed, height is 40 mm. Reproduced with permission.<sup>[137]</sup> Copyright 2015, Wiley-VCH. c) Polyjet-printed molds used to cast helical 3D structures in (b). d) Sharkskin-inspired magnetically reconfigurable acoustic structures being used to construct acoustic logic gates. Each pillar has a diameter of 1.5 cm and a height of 4.25 cm. “A” and “B” denote inputs, whereas “C” is the output, in red. Figure shows an (i) AND gate and (ii) OR gate. Reproduced under terms of the CC-BY license.<sup>[138]</sup> Copyright 2020, The Authors, published by AAAS.

lattice mold, to produce a structure that could switch between singly-negative or doubly-negative operation modes. The mold was fabricated using projection micro-SLA, a type of printing technology modified for microfabrication.

3D-printed molds<sup>[139]</sup> can effectively cast elastomeric structures, whereby mechanical buckling would modulate the stiffness of deformable elements to open and close bandgaps.<sup>[140]</sup> Such acoustic switching behavior was demonstrated in entirely soft 3D helical structures (Figure 5b). Here, polyjet-printed molds cast vinylpolysiloxane elastomers (Figure 5c).<sup>[137]</sup> Using FDM-printed molds, magnetoactive sharkskin-inspired AMMs were fabricated and magnetically configured into acoustic logic gates (Figure 5d).<sup>[138]</sup> The same limitations in 3D printing technologies apply when printing a mold, directly affecting the cast structure. For example, a 3D-printed mold with a poor surface finish would likely cast an object with a nonuniform surface profile. The degree of adhesion of the cured material with the mold is another aspect to consider. Moreover, conventional 3D-printed molds are unlikely to provide sufficient resolution for AMMs and PCs in the megahertz and gigahertz range. Soft lithography is more suitable in such cases.

We also see unique fabrication strategies utilizing simple objects for molding, demonstrated in the experimental realization of a nonperiodic AMM exhibiting dipolar resonance and a negative mass density. In this example, circular petri dishes cast suspended tungsten carbide (WC) beads (diameter, 397 or 500  $\mu\text{m}$ ) within epoxy resin.<sup>[141]</sup> The casting and curing

process was repeated multiple times, with each layer of resin containing a random dispersion of WC particles (2–10% volume fraction). Repetitive casting and curing present a new opportunity to fabricate layered AMM and PC designs, exploiting the versatility of silicones and resins with each layer characterized by different properties.

### 4.3. Microfluidics and Wet-Chemical Techniques

Microfluidics deals with the precise control of fluids in volumes of micro/nanoliters or less. A possible application of microfluidic techniques is the fabrication of porous microspheres, which can manipulate acoustic wave propagation within a fluid medium. There is a class of soft AMMs, designed to consist of a random dispersion of porous microparticles, which behave as slow soft Mie resonators. These suspended resonators form an AMM that exhibits a negative bulk modulus and macroscopic isotropy. A possible fabrication technique used to create microspheres is high-internal-phase-emulsion (HIPE) templating.<sup>[142]</sup> This procedure was conducted by a microfluidic device for in situ polymerization, producing soft porous PDMS microspheres (Figure 6b).<sup>[133,143]</sup> Besides microspheres, HIPE templating was also recently used to fabricate a soft, porous GRIN metasurface (Figure 6a).<sup>[144]</sup> The broadband ultrasonic metasurface could shape 3D wavefronts underwater, allowing acoustic focusing (200 kHz) and the generation of vortices (150 kHz).

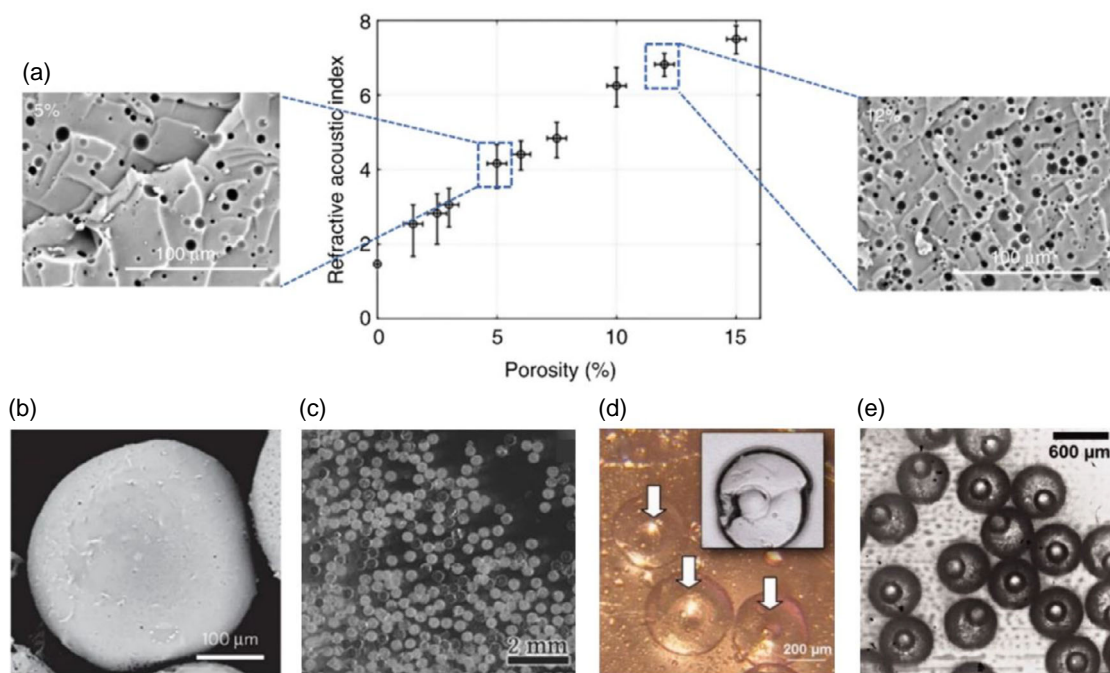


**Figure 6.** Different structures fabricated using microfluidic techniques. a) Acoustic refractive index measured against porosities of silicone rubber. SEM images show porosities of 5% (left) and 12% (right). The GRIN metasurface was fabricated by HIPE templating. Reproduced under terms of the CC-BY license.<sup>[144]</sup> Copyright 2019, The Authors, published by Springer Nature Limited. b) Polydimethylsiloxane (PDMS) microspheres fabricated by HIPE templating. Reproduced with permission.<sup>[133]</sup> Copyright 2015, Springer Nature Limited. c) Silica xerogel beads fabricated via the sol–gel method, dispersed within a carbopol matrix. Reproduced with permission.<sup>[134]</sup> Copyright 2015, Wiley-VCH. d) Core–shell particles fabricated by the first method, through temperature-controlled gelation, and the e) second method, through in situ UV polymerization and a complexation reaction. Reproduced with permission.<sup>[145]</sup> Copyright 2012, Wiley Periodicals, Inc.

Another way to fabricate porous microspheres for acoustic resonance is via the sol–gel method, a type of wet-chemical technique. For instance, silica xerogel beads were synthesized by means of digital microfluidics, where the precursor and catalyst reacted together within the microchannel to form droplets within a continuous stream of fluorinated oil. The beads were washed and dried in ethanol, followed by plasma oxidation for random distribution into a caropol polymer matrix (Figure 6c).<sup>[34]</sup> The resulting colloidal metamaterial exhibited frequency bands with a negative acoustic refractive index.

Apart from porous microparticles, core–shell particles can also act as locally resonant mechanical oscillators. Two decades ago, a locally resonant sonic crystal was fabricated for the first time, with the use of periodically arranged core–shell particles, having a lattice constant of 1.55 cm.<sup>[146]</sup> It was observed that the bandgap phenomena using silicone-coated lead spheres only existed for soft, rather than rigid, coatings. A few years later, coated spheres that distributed either randomly or periodically, in a matrix, were investigated analytically, where the proposed composite structures exhibited low-frequency (375–1335 Hz) bandgaps at resonant frequencies.<sup>[147]</sup> More recently, based on the same analytical model, core–shell microspheres for a nonperiodic AMM with a negative mass density were experimentally demonstrated.<sup>[145]</sup> This time, the core–shell particles were significantly reduced in size for operation in the ultrasonic regime. Due to the miniaturization of these composite particles, fabrication was not a straightforward task.

Two different methods, both via microfluidic manipulation, were presented.<sup>[145]</sup> The first method (Figure 6d) used temperature-controlled gelation to encapsulate solid polymethylmethacrylate (PMMA) core particles. Agarose droplets were dispensed into the microchannel using silicone oil as a carrier fluid to form the hydrogel coating. The second method (Figure 6e) instead used a liquid core made from ethylene glycol dimethacrylate (EGDA) droplets, which solidified through in situ UV polymerization after encapsulation. The shell-coating gelation was conducted using a complexation reaction by calcium cross-linking. While gelation-based approaches are proficient in microsphere synthesis, it can be a time-consuming process. In the discussed examples, the successful cross-disciplinary integration of technologies was showcased utilizing fluid-mechanical processes to build acoustic structures.

## 5. Arrangement and Assembly Methods

Theoretical models can determine the configurations or assemblies in which AMMs and PCs are put together, and there are several approaches to achieve them physically. Bonding through the use of adhesives, such as glues and epoxies, is an accessible method to fabricate heterogeneous (e.g., membrane-type structures) or homogenous<sup>[43]</sup> structures. For example, Popa and Cummer<sup>[148]</sup> developed a nonreciprocal and highly nonlinear AMM consisting of a thin piezoelectric membrane (PZM) bonded between Helmholtz cavities, as an actively controlled unidirectional metamaterial (isolation factor > 10 dB). The Helmholtz resonators were tuned to different frequencies to create asymmetry, whereas a nonlinear electronic circuit drove the PZM that reversibly converted electrical and acoustic energy.

Another design modified a Helmholtz cavity by gluing a polyvinylidene fluoride (PVDF) patch with magnetic blocks onto an aluminum membrane. Acrylic plates were mechanically fastened together using bolts to construct the resonator for sound insulation (Figure 7a) and energy-harvesting applications.<sup>[18]</sup>

A major advantage of using adhesives is the ability to bond different types of materials together. Other membrane-type AMMs have bonded material layers such as polycarbonate and porous fiberglass wool (Figure 7b),<sup>[39]</sup> polyurethane and plastic,<sup>[26]</sup> or latex rubber on aramid fiber sheets.<sup>[151]</sup> Besides membranes, this assembly technique was also utilized over a range of other AMM and PC design types. These include examples like reconfigurable origami modules and lattices<sup>[45,46]</sup> and a PC plate with arrays of cylindrical piezoelectric resonators.<sup>[152]</sup> It is noteworthy that the handling and alignment of small structures can be challenging when conducted manually. Even for larger structures, the presence of glue and misalignment can impact acoustic performance. For this very reason, the beam-focusing experimental frequency (81 kHz) for the stacked foam-like metallic PC<sup>[112]</sup> discussed in an earlier section (Section 3.2, Figure 3b) deviated from the theoretical value (71.2 kHz). In addition, bonding nanoscale AMM and PC structures operating in the hypersonic regime (>100 MHz) would require other specialized techniques like anodic or vacuum bonding as an alternative to conventional adhesives.

Particularly for 3D-printed structures, adhesives can also help to reduce the burden of postprocessing. The 3D Luneburg lens (Figure 7c)<sup>[62]</sup> discussed in an earlier section (Section 3.1) was printed as two separate hemispheres, before being bonded together via UV irradiation. A main reason for the bonding step was to minimize the use of support structures. In an isotropic spherical space-coiling device,<sup>[43]</sup> the entire ball was composed of seven glued parts, each with identical labyrinthine channels (Figure 7e). Here, the primary purpose of using adhesives was to allow sound waves to enter the structure and freely propagate through the channels. However, in doing so, the water-soluble support material could be more easily removed in each part before the complete AMM was assembled. This strategy is a simple and effective method to bring together 3D-printed parts to form AMM and PC structures with complex internal geometries.

Rather than being randomly dispersed as discussed in the previous section (Section 4.3), microspheres can be ordered or disordered in a certain manner, through several self-assembly strategies. One such strategy is acoustic levitation. This scheme was showcased in a PC created from the colloidal suspension of polystyrene spheres in water.<sup>[32]</sup> Piezoceramic transducers levitated the spheres to assume different lattice configurations, excited at the frequencies of 2.25, 3.75, and 5.25 MHz. Besides demonstrating contactless tunability, few reconfigurable PCs had periodicities corresponding to such high frequencies. However, when levitating spherical objects through the use of a standing wave field, the size is often limited to no more than half the wavelength. Furthermore, levitated objects are ideally symmetrical. It is challenging to levitate larger sizes and different shapes, requiring other techniques such as twin traps and vortices.<sup>[153–155]</sup>

If not assembled within a liquid medium, self-assembly can be utilized at the air–water interfaces. Such designs typically operate through contact resonance of the spheres with the substrate. The Langmuir–Blodgett technique is a prevailing method for the



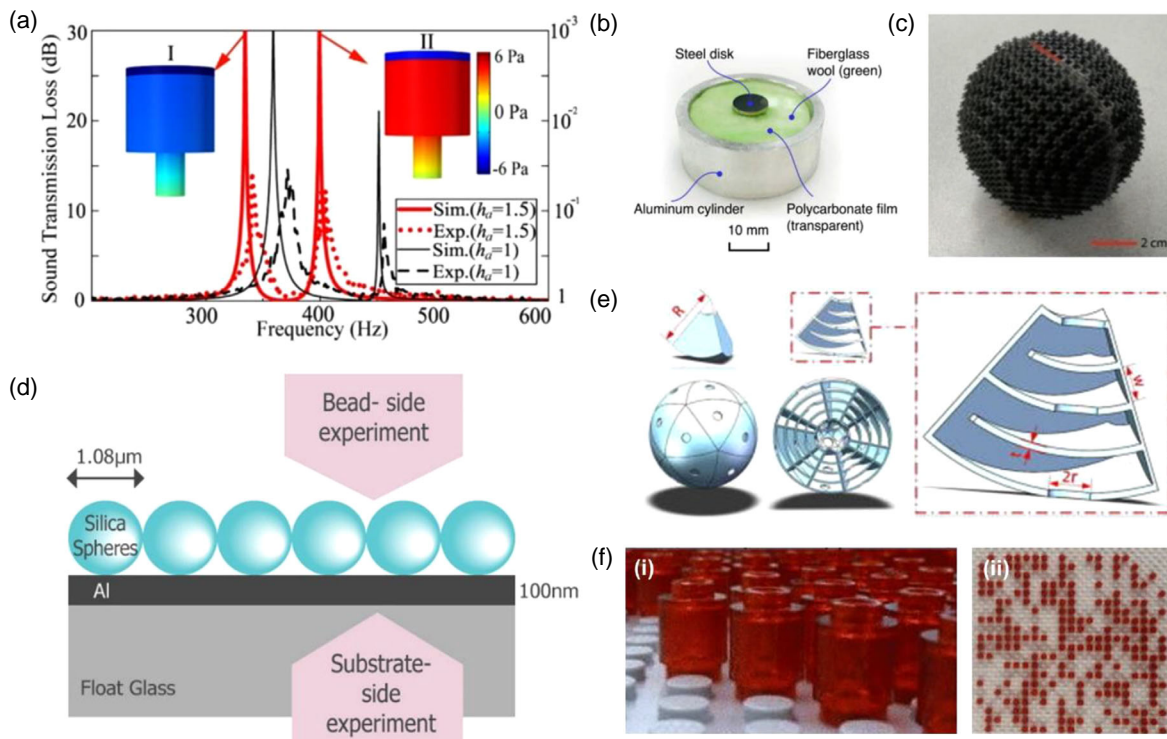


**Figure 7.** Assembled AMM and PC structures. a) Simulated and experimental results of sound transmission loss in dB (left axis) and the acoustic transmission factor (right axis) showing sound insulation effects. Rigid masses have thicknesses,  $h_a = 1.5$  and 1 mm. Reproduced with permission.<sup>[18]</sup> Copyright 2018, IOP Publishing Ltd. b) Layered membrane-type AMM for absorption and broadband insulation. Reproduced with permission.<sup>[39]</sup> Copyright 2018, AIP Publishing LLC. c) Acoustic Luneburg lens. Reproduced under terms of the CC-BY license.<sup>[62]</sup> Copyright 2018, The Authors, published by Springer Nature Limited. d) Monolayer of silica spheres assembled using the wedge-shaped cell convective technique. The aluminum (Al) film coating has a thickness of 100 nm. Reproduced under terms of the CC-BY license.<sup>[149]</sup> Copyright 2018, The Authors, published by IOP Publishing Ltd on behalf of Deutsche Physikalische Gesellschaft. e) Isotropic spherical space-coiling device,  $R = 35$  mm. Magnified labyrinthine part shows channel, where  $t = 1$  mm,  $r = 3$  mm, and  $w = 5$  mm. Reproduced with permission.<sup>[43]</sup> Copyright 2017, AIP Publishing LLC. f) (i) Lego® bricks assembled onto the acrylonitrile butadiene styrene (ABS) baseplate via interference fitting. (ii) A random arrangement of 210 bricks, which maintained a low-frequency bandgap of 2.2 kHz. Reproduced with permission.<sup>[150]</sup> Copyright 2015, AIP Publishing LLC.

fabrication of molecular monolayers, adapted for the monolayer deposition of spheres. It was demonstrated in the assembly of disordered polystyrene microspheres (1.02  $\mu\text{m}$ , diameter) over a soda-lime glass substrate coated with aluminum, with the monolayer subsequently removed by a microcontact printing technique.<sup>[156]</sup> Sound attenuation of SAW waves was achieved at  $\approx 240$  MHz, through Hertzian contact resonance with the spheres. A different AMM used a similar setup using a silicon substrate, to observe the hybridization phenomena of the fundamental flexural Lamb wave mode.<sup>[157]</sup> Another self-assembly method is the wedge-shaped cell convective technique, implemented to build an AMM for gigahertz imaging capabilities, also exploiting contact mechanics (Figure 7d).<sup>[149]</sup> These examples show how self-assembly techniques can transform random colloidal dispersions into functional AMMs or PCs for acoustic applications.

Interference fitting, or press fitting, is a method of fastening objects together by means of friction. Lego® is a well-known example of simple and robust interference fitting, which was exploited for fabricating a PC.<sup>[150]</sup> Cylindrical bricks were assembled and fit into different topological patterns without the use of adhesives, onto an ABS platform (Figure 7f). Definite bandgaps were observed from 1.8 to 2.6 and 5.5 to 11 kHz. This versatile

scheme was again seen in the fabrication of a porous AMM, where rigid plates were inserted into melamine foams for sound-absorptive properties.<sup>[158]</sup> The topological pyrochlore lattice<sup>[60]</sup> discussed in an earlier section (Section 3.1, Figure 2c) used a different technique called snap-fitting. Snap-fitting involves the momentary deflection of the protruded feature of one object as it is inserted into and interlocked with the depressed feature of another object. Due to this deflection, this method is not ideal for constant reassembly, risking damage to the components.

Purely through strategic arrangement, soda cans have proven to be surprisingly effective acoustic elements (Helmholtz resonators) that can exhibit graphene-like dispersion or achieve super lensing when placed in a honeycomb configuration.<sup>[3,159]</sup> Graphene-like Dirac dispersion was achieved with a double soda can lattice resonating at separate frequencies. The second sublattice was composed of resonant defects which behaved as subwavelength cavities, mimicking the tight-binding-governed Hamiltonians of graphene. It is remarkable that such low-cost and accessible commonplace objects can be collectively combined using smart theoretical design and strategic assembly for meaningful acoustic wave manipulation.

## 6. Conclusion and Outlook

Our discussions of the enlisted fabrication and assembly techniques took us through different examples and strategies for building AMMs and PCs. It often involves a delicate balance between specific building requirements (e.g., geometry, materials) and the limitations of each method, keeping in view the factors of accessibility, time, cost, and quality. The operating frequency of the device can also significantly widen or narrow down the scope of suitable methods. **Figure 8** shows fabrication processes and technologies appropriate for designing AMMs and PCs which generally occupy specific operating frequency ranges within the phononic spectrum.

Based on the examined techniques, we also synthesize a broad visual map, highlighting examples from the recent literature dealing with building active and passive, micro- and macro-AMM and PC designs (**Figure 9**). Colored blocks marked with crosses denote possible untapped combinations, uncovering and inspiring future opportunities for research.

There are still many unexplored paradigms that can offer increasingly creative solutions to build AMMs and PCs, as researchers continue to push for unusual, groundbreaking acoustic devices. For example, based on the discussed single-step fabrication techniques, we have observed that despite being able to print an impressive catalogue of materials, DIW has been underutilized in fabricating acoustic devices. DIW has fabricated ceramic-based PCs and graphene aerogels, providing a clear indication of the ability to print porous structures. This technique could help develop printable colloidal particles with high porosity. Moreover, DIW can print LCEs, useful for responsive and programmable actuation. Periodic lattices, membrane-type, or

origami-based LCE structures could morph or deform on demand, actively modulating the transmission of acoustic waves. Alternatively, SLA or DLP printing can help to integrate channels for actuating foldable structures using fluidic or pneumatic control. Subsequently, automated microfluidic logic<sup>[163]</sup> could be applied for active computational designs.

Besides being able to cut out elaborate shapes and patterns as a thermal machining process, a conventional CO<sub>2</sub> laser can also be used to create graphene foam. Laser-induced graphene (LIG) was showcased recently to not only be able to act as a sound source, but also as an acoustic sensor, with thicknesses in the range of microns.<sup>[164]</sup> Using LIG coatings, AMMs and PCs could exploit the same capabilities in combination with directing or focusing sound. In addition to graphene-based coating, the integration of thin-film electronics can support smarter, compact, and portable metasurfaces. Another interesting application is the synthesis of metallic nanoparticles using  $\mu$ -EDM. If these particles are ferromagnetic, they could be collectively suspended within a fluid medium as tunable assemblies in response to external magnetic stimuli.

Under multi-step fabrication, microfabrication techniques can be further developed for higher-frequency AMMs in the megahertz-to-terahertz range, which are limited in current literature. Hybrid micromachining and microfabrication processes can help to achieve this with the fabrication of MEMS- and nanoelectromechanical (NEMS)-based designs. Two-photon lithography has enabled the direct fabrication of 3D nanostructures. This method could be adapted to create colloidal particles of both spherical and nonspherical shapes, which could later be self-assembled in different configurations. In addition, two-photon lithography, together with other processes such as sputtering,

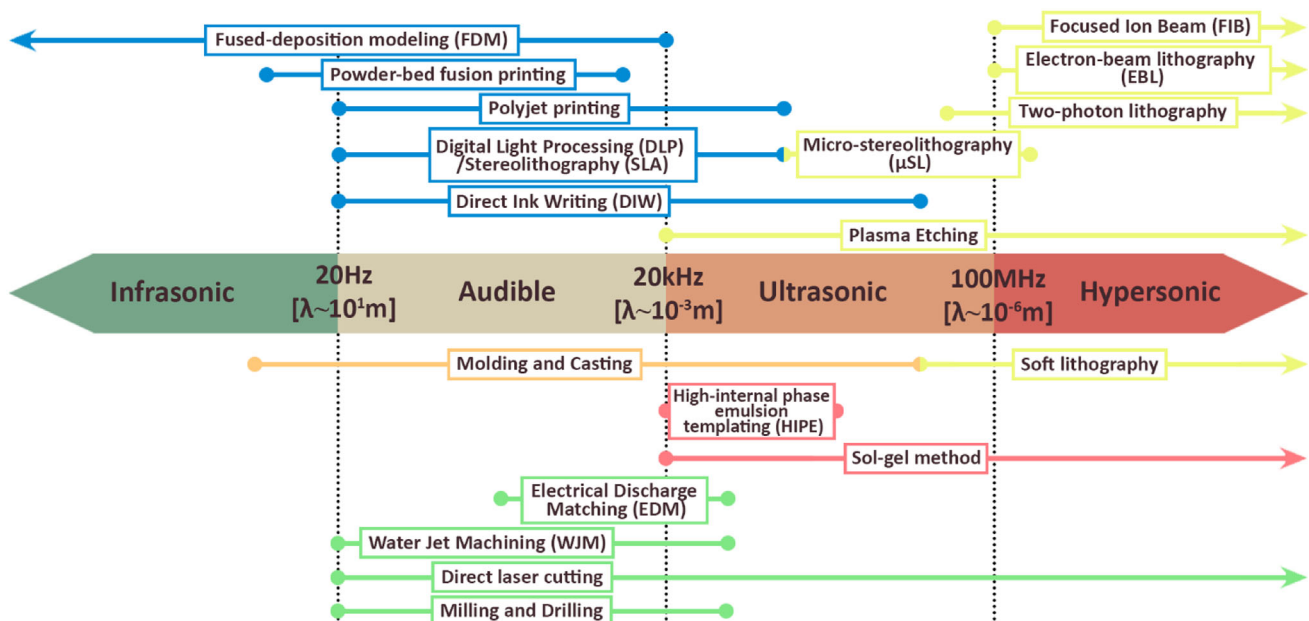


**Figure 8.** Phononic spectrum showing the fabrication methods for various operating frequency ranges for AMMs and PCs. The color schemes for the lines and boxes denote the type of fabrication method. Blue refers to “3D printing,” green refers to “machining,” yellow refers to “microfabrication,” orange refers to “molding and casting,” and coral pink refers to “microfluidics and wet-chemical techniques.”  $\lambda$  refers to the order of the wavelength of the listed frequency.

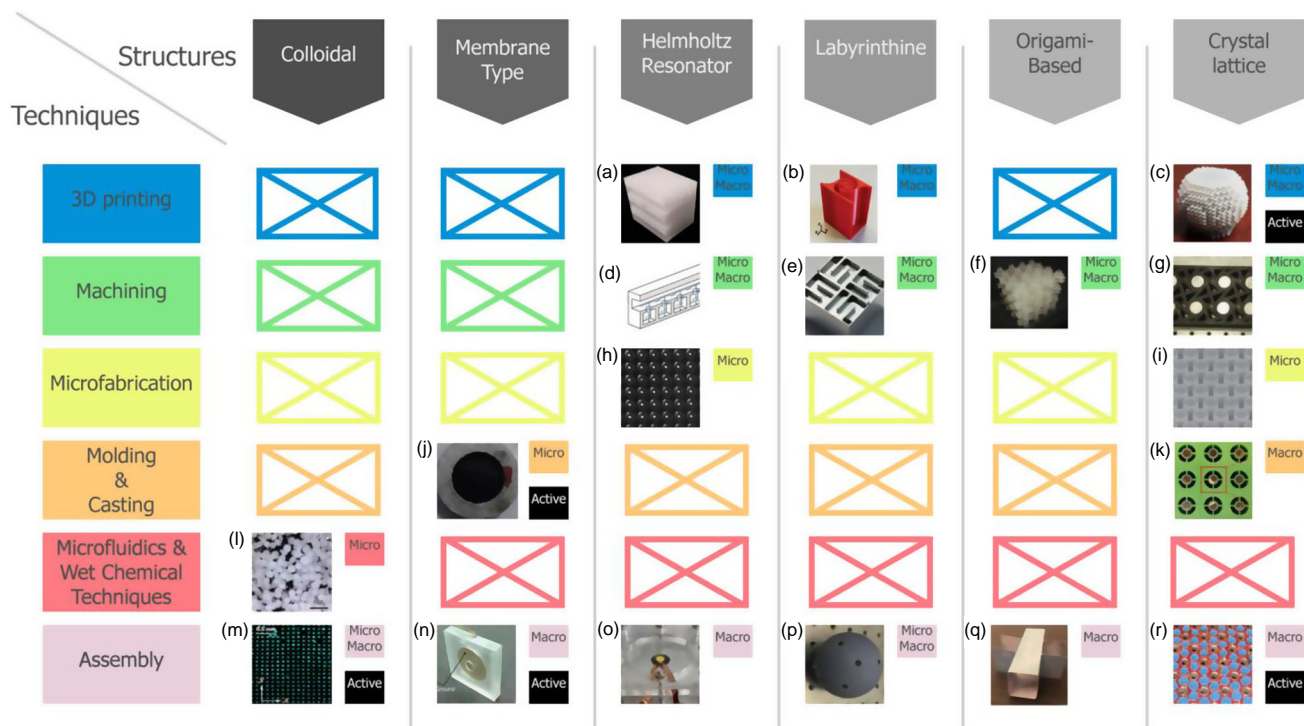


**Figure 9.** A visual map of techniques and six highlighted AMM and PC structure types. 3D printing of a) Helmholtz resonators<sup>[37,72,73,86]</sup> (Image reproduced under terms of the CC-BY license.<sup>[86]</sup> Copyright 2017, The Authors, published by Springer Nature Limited), b) labyrinthine structures<sup>[1,5,42,43,74,93,95,96,160,161]</sup> (Image reproduced with permission.<sup>[74]</sup> Copyright 2013, AIP Publishing LLC), and c) crystal lattice structures<sup>[40,60,62,76,82,83,84,94,97,98,103,104,162]</sup> (Image reproduced with permission.<sup>[84]</sup> Copyright 2020, AIP Publishing LLC). Machining of d) Helmholtz resonators,<sup>[35]</sup> e) labyrinthine structures<sup>[75]</sup> (Reproduced with permission.<sup>[75]</sup> Copyright 2013, AIP Publishing LLC), f) origami-based structures<sup>[44]</sup> (Adapted under terms of the CC-BY license.<sup>[44]</sup> Copyright 2016, The Authors, published by AAAS), and g) crystal lattice structures<sup>[53,57,64,108,109,111–112,113]</sup> (Image reproduced with permission.<sup>[115]</sup> Copyright 2013, Elsevier B.V.). Microfabrication of h) Helmholtz resonators<sup>[36]</sup> (Reproduced with permission.<sup>[36]</sup> Copyright 2013, AIP Publishing LLC.) and i) crystal lattice structures<sup>[41,63,70,124,125]</sup> (Image reproduced with permission.<sup>[70]</sup> Copyright 2016, American Physical Society). Molding & Casting of j) membrane-type structures<sup>[38]</sup> (Reproduced with permission.<sup>[38]</sup> Copyright 2014, AIP Publishing LLC), and k) crystal lattice structures<sup>[48,137,140]</sup> (Image reproduced with permission.<sup>[140]</sup> Copyright 2014, American Physical Society). Microfluidics and wet-chemical techniques for l) colloidal<sup>[33,34,145]</sup> structures (Image reproduced with permission.<sup>[33]</sup> Copyright 2015, Springer Nature Limited). Assembly of m) colloidal<sup>[32]</sup> (Reproduced with permission.<sup>[32]</sup> Copyright 2016, AAAS), n) membrane-type structures<sup>[18,26,38,39,148,151]</sup> (Image reproduced with permission.<sup>[148]</sup> Copyright 2014, Springer Nature Limited), o) Helmholtz resonators<sup>[18,148]</sup> (Image reproduced with permission.<sup>[18]</sup> Copyright 2018, IOP Publishing Ltd.), p) labyrinthine structures<sup>[43,75]</sup> (Image reproduced with permission.<sup>[43]</sup> Copyright 2017, AIP Publishing LLC), q) origami-based structures<sup>[44–46]</sup> (Image reproduced with permission.<sup>[46]</sup> Copyright 2019, American Physical Society), and r) crystal lattice structures<sup>[3,32,152,156,157,159]</sup> (Image reproduced under terms of the CC-BY license.<sup>[159]</sup> Copyright 2017, The Authors, published by Springer Nature Limited). To the right-hand side of the images, small colorful text boxes denote “microstructure” or “macrostructure” classification while small black boxes indicate active structures. Larger colorful boxes with crosses show possible unexplored combinations for future research.

can fabricate novel electrical, thermal, or chemomechanical<sup>[165]</sup> actively tunable microlattices to control bandgap formation. By drawing inspiration from mechanical metamaterial<sup>[166]</sup> fabrication, deformable polymer microlattices are also possible through 3D laser microprinting.<sup>[167]</sup> Moreover, lithography-based folding approaches, or 4D printing with shape memory polymers, may be adapted to create millimeter-to-micrometer-scale origami or labyrinthine structures<sup>[168]</sup> for acoustics.

Molding and casting with sacrificial templates is a powerful method that could cast complex architectures which are difficult to print directly. Microfluidic-based elastomeric or hydrogel<sup>[169]</sup> networks can be fabricated for building soft, controllable AMMs and PCs. Hydrogel-based structures with embedded nanoparticles<sup>[170]</sup> can also be further developed for impedance matching and enhanced acoustic performance for applications like underwater cloaking. Besides using HIPE templating for fabricating

porous structures, salt can be printed and sintered as a template before leaching, to cast microscaffolds with ordered porosity.<sup>[171]</sup> Endless possibilities await the burgeoning fields of AMMs and PCs. As they continue to mature and transition from theory to reality, alongside advancements in fabrication, they are set to transform the way we live, experience, and interact with sound.

## Acknowledgements

C.C. and S.B. contributed equally to this work. The authors would like to thank Mr. Tom Williams and Mr. Eimontas Jankauskis for their support in creating the figures and illustrations. This work was supported by EU's H2020 program through their ERC Advanced Grant (number 787413) and the Royal Academy of Engineering through their Chairs in Emerging Technology Program. The authors declare no competing interests.



## Conflict of Interest

The authors declare no conflict of interest.

## Keywords

acoustic metamaterials, fabrication methods, microfabrication, phononic crystals

Received: August 21, 2020

Revised: October 3, 2020

Published online: November 9, 2020

- [1] B. Yuan, Y. Cheng, X. Liu, *Appl. Phys. Express* **2015**, *8*, 027301.
- [2] Y. X. Shen, Y. G. Peng, F. Cai, K. Huang, D. G. Zhao, C. W. Qiu, H. Zheng, X. F. Zhu, *Nat. Commun.* **2019**, *10*, 1.
- [3] N. Kaina, F. Lemoult, M. Fink, G. Lerosey, *Nature* **2015**, *525*, 77.
- [4] L. Zigoneanu, B.-I. Popa, S. A. Cummer, *Nat. Mater.* **2014**, *13*, 352.
- [5] G. Memoli, M. Caleap, M. Asakawa, D. R. Sahoo, B. W. Drinkwater, S. Subramanian, *Nat. Commun.* **2017**, *8*, 14608.
- [6] K. Melde, A. G. Mark, T. Qiu, P. Fischer, *Nature* **2016**, *537*, 518.
- [7] Y. Zhu, J. Hu, X. Fan, J. Yang, B. Liang, X. Zhu, J. Cheng, *Nat. Commun.* **2018**, *9*, 1632.
- [8] J. Prat-Camps, G. Christopoulos, J. Hardwick, S. Subramanian, *Adv. Mater. Technol.* **2020**, *5*, 2000041.
- [9] D. Zhao, Y.-T. Wang, K.-H. Fung, Z.-Q. Zhang, C. T. Chan, *Phys. Rev. B* **2020**, *101*, 054107.
- [10] D. Lee, M. Kim, J. Rho, *J. Phys.: Condens. Matter* **2019**, *31*, 375901.
- [11] V. E. Gusev, O. B. Wright, *New J. Phys.* **2014**, *16*, 123053.
- [12] A. Souslov, B. C. Van Zuijden, D. Bartolo, V. Vitelli, *Nat. Phys.* **2017**, *13*, 1091.
- [13] Y. Zhao, H. Y. Dong, S. Zhao, S. Min, J. Cheng, B. Li, F. Chi, S. Liu, *J. Appl. Phys.* **2019**, *126*, 065103.
- [14] R. Ghaffarivardavagh, J. Nikolajczyk, S. Anderson, X. Zhang, *Phys. Rev. B* **2019**, *99*, 024302.
- [15] J. Han, S. Tang, R. Wang, W. Wang, *AIP Adv.* **2019**, *9*, 065201.
- [16] C. Shen, Y. Xie, N. Sui, W. Wang, S. A. Cummer, Y. Jing, *Phys. Rev. Lett.* **2015**, *115*, 254301.
- [17] S. Qi, M. Oudich, Y. Li, B. Assouar, *Appl. Phys. Lett.* **2016**, *108*, 263501.
- [18] X. Zhang, H. Zhang, Z. Chen, G. Wang, *Smart Mater. Struct.* **2018**, *27*, 105018.
- [19] O. Georgiou, H. Limerick, L. Corenthy, M. Maksymenko, S. Frish, J. R. Kim, M. Perry, J. Müller, M. Bachynskyi, in *Conf. Hum. Factors Comput. Syst. – Proc.*, Association for Computing Machinery, New York, NY **2019**, pp. 1–9.
- [20] T. Chen, J. Liu, K. Zhu, T. Waliczky, in *SIGGRAPH Asia 2017 VR Showcase, SA 2017*, Association for Computing Machinery, Inc, New York, NY **2017**, pp. 1–2.
- [21] J. Albouys-Perrois, J. Laviole, C. Briant, A. M. Brock, in *Conf. Hum. Factors Comput. Syst. – Proc.*, Association for Computing Machinery, New York, NY **2018**, pp. 1–14.
- [22] C. T. Vi, D. Ablart, E. Gatti, C. Velasco, M. Obrist, *Int. J. Hum. Comput. Stud.* **2017**, *108*, 1.
- [23] G. Memoli, L. Chisari, J. P. Eccles, M. Caleap, B. W. Drinkwater, S. Subramanian, in *Conf. Hum. Factors Comput. Syst. – Proc.*, Association For Computing Machinery, New York, NY **2019**, pp. 1–14.
- [24] R. Hirayama, D. Martinez Plasencia, N. Masuda, S. Subramanian, *Nature* **2019**, *575*, 320.
- [25] M. A. Norasikin, D. Martinez Plasencia, S. Polychronopoulos, G. Memoli, Y. Tokuda, S. Subramanian, in *31st Annu. ACM Symp. User Interface Softw. Technol. – UIST '18*, ACM Press, New York, NY **2018**, pp. 247–259.
- [26] G. Ma, X. Fan, P. Sheng, M. Fink, *Proc. Natl. Acad. Sci.* **2018**, *115*, 6638.
- [27] Y. Li, S. Wang, Q. Peng, Z. Zhou, Z. Yang, X. He, Y. Li, *Nanoscale* **2019**, *11*, 16384.
- [28] M. R. Haberman, M. D. Guild, *Phys. Today* **2016**, *69*, 42.
- [29] B. Liang, J. Cheng, C.-W. Qiu, *Nanophotonics* **2018**, *7*, 1191.
- [30] B. Assouar, B. Liang, Y. Wu, Y. Li, J.-C. Cheng, Y. Jing, *Nat. Rev. Mater.* **2018**, *3*, 460.
- [31] G. Ma, P. Sheng, *Sci. Adv.* **2016**, *2*, e1501595.
- [32] M. Caleap, B. W. Drinkwater, *Proc. Natl. Acad. Sci.* **2014**, *111*, 6226.
- [33] T. Brunet, A. Merlin, B. Mascaro, K. Zimny, J. Leng, O. Poncelet, C. Aristégui, O. Mondain-Monval, *Nat. Mater.* **2015**, *14*, 384.
- [34] S. Raffy, B. Mascaro, T. Brunet, O. Mondain-Monval, J. Leng, *Adv. Mater.* **2016**, *28*, 1760.
- [35] N. Fang, D. Xi, J. Xu, M. Ambati, W. Srituravanich, C. Sun, X. Zhang, *Nat. Mater.* **2006**, *5*, 452.
- [36] W. N. Yunker, C. B. Stevens, G. T. Flowers, R. N. Dean, *J. Appl. Phys.* **2013**, *113*, 024906.
- [37] X. Jiang, Y. Li, B. Liang, J. Cheng, L. Zhang, *Phys. Rev. Lett.* **2016**, *117*, 034301.
- [38] X. Chen, X. Xu, S. Ai, H. Chen, Y. Pei, X. Zhou, *Appl. Phys. Lett.* **2014**, *105*, 071913.
- [39] X. Wang, X. Luo, H. Zhao, Z. Huang, *Appl. Phys. Lett.* **2018**, *112*, 021901.
- [40] T. Grabec, M. Koller, P. Sedlák, A. Kruisová, B. Román-Manso, M. Belmonte, P. Miranzo, H. Seiner, *Wave Motion* **2020**, *92*, 102417.
- [41] N. Wang, J. M.-L. Tsai, F.-L. Hsiao, B. W. Soon, D.-L. Kwong, M. Palaniapan, C. Lee, *J. Microelectromech. Syst.* **2012**, *21*, 801.
- [42] S. K. Maurya, A. Pandey, S. Shukla, S. Saxena, *Sci. Rep.* **2016**, *6*, 33683.
- [43] X. F. Fu, G. Y. Li, M. H. Lu, G. Lu, X. Huang, *Appl. Phys. Lett.* **2017**, *111*, 251904.
- [44] S. Babaee, J. T. B. Overvelde, E. R. Chen, V. Tournat, K. Bertoldi, *Sci. Adv.* **2016**, *2*, e1601019.
- [45] H. Fang, X. Yu, L. Cheng, *Smart Mater. Struct.* **2018**, *27*, 095007.
- [46] Y. Zhu, F. Fei, S. Fan, L. Cao, K. Donda, B. Assouar, *Phys. Rev. Appl.* **2019**, *12*, 034029.
- [47] S. A. Cummer, J. Christensen, A. Alù, *Nat. Rev. Mater.* **2016**, *1*, 16001.
- [48] K. Yu, N. X. Fang, G. Huang, Q. Wang, *Adv. Mater.* **2018**, *30*, 1706348.
- [49] M. Thota, K. W. Wang, *J. Appl. Phys.* **2017**, *122*, 154901.
- [50] G. Ma, M. Yang, S. Xiao, Z. Yang, P. Sheng, *Nat. Mater.* **2014**, *13*, 873.
- [51] C. He, X. Ni, H. Ge, X. C. Sun, Y. Bin Chen, M. H. Lu, X. P. Liu, Y. F. Chen, *Nat. Phys.* **2016**, *12*, 1124.
- [52] Y.-G. Peng, C.-Z. Qin, D.-G. Zhao, Y.-X. Shen, X.-Y. Xu, M. Bao, H. Jia, X.-F. Zhu, *Nat. Commun.* **2016**, *7*, 13368.
- [53] J. Lu, C. Qiu, L. Ye, X. Fan, M. Ke, F. Zhang, Z. Liu, *Nat. Phys.* **2017**, *13*, 369.
- [54] Z. Tian, C. Shen, J. Li, E. Reit, H. Bachman, J. E. S. Socolar, S. A. Cummer, T. Jun Huang, *Nat. Commun.* **2020**, *11*, 1.
- [55] F. Li, X. Huang, J. Lu, J. Ma, Z. Liu, *Nat. Phys.* **2018**, *14*, 30.
- [56] H. He, C. Qiu, L. Ye, X. Cai, X. Fan, M. Ke, F. Zhang, Z. Liu, *Nature* **2018**, *560*, 61.
- [57] H. Xue, Y. Yang, F. Gao, Y. Chong, B. Zhang, *Nat. Mater.* **2019**, *18*, 108.
- [58] X. Zhang, B.-Y. Xie, H.-F. Wang, X. Xu, Y. Tian, J.-H. Jiang, M.-H. Lu, Y.-F. Chen, *Nat. Commun.* **2019**, *10*, 5331.
- [59] H. Xue, Y. Yang, G. Liu, F. Gao, Y. Chong, B. Zhang, *Phys. Rev. Lett.* **2019**, *122*, 244301.
- [60] M. Weiner, X. Ni, M. Li, A. Alù, A. B. Khanikaev, *Sci. Adv.* **2020**, *6*, eaay4166.

- [61] Z. Zhang, Y. Tian, Y. Cheng, Q. Wei, X. Liu, J. Christensen, *Phys. Rev. Appl.* **2018**, 9, 034032.
- [62] Y. Xie, Y. Fu, Z. Jia, J. Li, C. Shen, Y. Xu, H. Chen, S. A. Cummer, *Sci. Rep.* **2018**, 8, 16188.
- [63] M.-J. Chiou, Y.-C. Lin, T. Ono, M. Esashi, S.-L. Yeh, T.-T. Wu, *Ultrasonics* **2014**, 54, 1984.
- [64] S. A. R. Kuchibhatla, P. Rajagopal, *NDT E Int.* **2019**, 102, 304.
- [65] K. Li, Y.-G. Peng, X.-F. Zhu, J.-T. Zhang, H.-J. Lv, S.-C. Liu, *Appl. Phys. Lett.* **2014**, 104, 043505.
- [66] A. Zhao, Z. Zhao, X. Zhang, X. Cai, L. Wang, T. Wu, H. Chen, *Appl. Phys. Lett.* **2017**, 110, 011907.
- [67] A. N. Norris, *J. Acoust. Soc. Am.* **2009**, 125, 839.
- [68] L. Shao, S. Maity, L. Zheng, L. Wu, A. Shams-Ansari, Y.-I. Sohn, E. Puma, M. N. Gadalla, M. Zhang, C. Wang, E. Hu, K. Lai, M. Lončar, *Phys. Rev. Appl.* **2019**, 12, 014022.
- [69] S. L. Yeh, Y. C. Lin, Y. C. Tsai, T. Ono, T. T. Wu, *Ultrasonics* **2016**, 71, 106.
- [70] D. Yudistira, A. Boes, B. Graczykowski, F. Alzina, L. Y. Yeo, C. M. Sotomayor Torres, A. Mitchell, *Phys. Rev. B* **2016**, 94, 094304.
- [71] D. Nardi, M. Travagliati, M. M. Murnane, H. C. Kapteyn, G. Ferrini, C. Giannetti, F. Banfi, *IEEE Sens. J.* **2015**, 15, 5142.
- [72] Y. Li, X. Jiang, B. Liang, J. Cheng, L. Zhang, *Phys. Rev. Appl.* **2015**, 4, 024003.
- [73] L. Zhao, S. Zhou, *Sensors* **2019**, 19, 788.
- [74] Y. Xie, A. Konneker, B.-I. Popa, S. A. Cummer, *Appl. Phys. Lett.* **2013**, 103, 201906.
- [75] T. Frenzel, J. David Brehm, T. Bückmann, R. Schittny, M. Kadic, M. Wegener, *Appl. Phys. Lett.* **2013**, 103, 061907.
- [76] E. R. Fotsing, A. Dubourg, A. Ross, J. Mardjono, *Appl. Acoust.* **2019**, 148, 322.
- [77] R. Zhu, X. N. Liu, G. K. Hu, C. T. Sun, G. L. Huang, *Nat. Commun.* **2014**, 5, 5510.
- [78] S. A. M. Tofail, E. P. Koumoulos, A. Bandyopadhyay, S. Bose, L. O'Donoghue, C. Charitidis, *Mater. Today* **2018**, 21, 22.
- [79] J. Zhao, Y. Zhang, X. Zhao, R. Wang, J. Xie, C. Yang, J. Wang, Q. Zhang, L. Li, C. Lu, Y. Yao, *Adv. Funct. Mater.* **2019**, 29, 1900809.
- [80] J. W. Boley, E. L. White, G. T.-C. Chiu, R. K. Kramer, *Adv. Funct. Mater.* **2014**, 24, 3501.
- [81] A. Kotikian, R. L. Truby, J. W. Boley, T. J. White, J. A. Lewis, *Adv. Mater.* **2018**, 30, 1706164.
- [82] A. Kruisová, H. Seiner, P. Sedlák, M. Landa, B. Román-Manso, P. Miranzo, M. Belmonte, *Appl. Phys. Lett.* **2014**, 105, 211904.
- [83] Z. Cai, S. Zhao, Z. Huang, Z. Li, M. Su, Z. Zhang, Z. Zhao, X. Hu, Y. Wang, Y. Song, *Adv. Funct. Mater.* **2019**, 29, 1906984.
- [84] L. Zhao, E. Laredo, O. Ryan, A. Yazdkhasti, H. T. Kim, R. Ganye, T. Horiuchi, M. Yu, *Appl. Phys. Lett.* **2020**, 116, 071902.
- [85] C. M. Park, S. H. Lee, *Appl. Phys. Lett.* **2018**, 112, 074101.
- [86] N. Jiménez, V. Romero-García, V. Pagneux, J.-P. Groby, *Sci. Rep.* **2017**, 7, 13595.
- [87] R. L. Truby, J. A. Lewis, *Nature* **2016**, 540, 371.
- [88] N. Bhattacharjee, C. Parra-Cabrera, Y. T. Kim, A. P. Kuo, A. Folch, *Adv. Mater.* **2018**, 30, 1800001.
- [89] D. K. Patel, A. H. Sakhaei, M. Layani, B. Zhang, Q. Ge, S. Magdassi, *Adv. Mater.* **2017**, 29, 1606000.
- [90] M. Wehner, R. L. Truby, D. J. Fitzgerald, B. Mosadegh, G. M. Whitesides, J. A. Lewis, R. J. Wood, *Nature* **2016**, 536, 451.
- [91] V. Peri, M. Serra-Garcia, R. Ilan, S. D. Huber, *Nat. Phys.* **2019**, 15, 357.
- [92] Z. Tian, C. Shen, J. Li, E. Reit, Y. Gu, H. Fu, S. A. Cummer, T. J. Huang, *Adv. Funct. Mater.* **2019**, 29, 1808489.
- [93] R. Ghaffarivardavagh, J. Nikolajczyk, R. Glynn Holt, S. Anderson, X. Zhang, *Nat. Commun.* **2018**, 9, 1349.
- [94] S. Ebrahimi-Nejad, M. Kheybari, *Mater. Res. Express* **2018**, 5, 105801.
- [95] S.-D. Zhao, A.-L. Chen, Y.-S. Wang, C. Zhang, *Phys. Rev. Appl.* **2018**, 10, 054066.
- [96] C. Zhang, X. Hu, *Phys. Rev. Appl.* **2016**, 6, 064025.
- [97] O. R. Bilal, A. Foehr, C. Daraio, *Adv. Mater.* **2017**, 29, 1700628.
- [98] K. H. Matlack, A. Bauhofer, S. Krödel, A. Palermo, C. Daraio, *Proc. Natl. Acad. Sci.* **2016**, 113, 8386.
- [99] Z. Wang, Z. Liu, C. Gao, K. Wong, S. Ye, Z. Xiao, *Surf. Coat. Technol.* **2020**, 387, 125122.
- [100] J. S. Chohan, R. Singh, K. S. Boparai, R. Penna, F. Fraternali, *Composites, Part B* **2017**, 117, 138.
- [101] Y. He, G. Xue, J. Fu, *Sci. Rep.* **2015**, 4, 6973.
- [102] S. Tol, F. L. Degertekin, A. Erturk, *Addit. Manuf.* **2019**, 29, 100780.
- [103] M. Reynolds, S. Daley, *Smart Mater. Struct.* **2014**, 23, 045030.
- [104] L. D'Alessandro, R. Ardito, F. Braghin, A. Corigliano, *Sci. Rep.* **2019**, 9, 8039.
- [105] A. Bergamini, M. Miniaci, T. Delpero, D. Tallarico, B. Van Damme, G. Hannema, I. Leibacher, A. Zemp, *Nat. Commun.* **2019**, 10, 1.
- [106] J. H. Martin, B. D. Yahata, J. M. Hundley, J. A. Mayer, T. A. Schaedler, T. M. Pollock, *Nature* **2017**, 549, 365.
- [107] J.-Y. Lee, J. An, C. K. Chua, *Appl. Mater. Today* **2017**, 7, 120.
- [108] V. M. García-Chocano, J. Christensen, J. Sánchez-Dehesa, *Phys. Rev. Lett.* **2014**, 112, 144301.
- [109] J. Zhu, J. Christensen, J. Jung, L. Martin-Moreno, X. Yin, L. Fok, X. Zhang, F. J. Garcia-Vidal, *Nat. Phys.* **2011**, 7, 52.
- [110] J. Li, L. Fok, X. Yin, G. Bartal, X. Zhang, *Nat. Mater.* **2009**, 8, 931.
- [111] Z. Tian, C. Shen, J. Li, E. Reit, H. Bachman, J. E. S. Socolar, S. A. Cummer, T. Jun Huang, *Nat. Commun.* **2020**, 11, 1.
- [112] A.-C. Hladky-Hennion, J. O. Vasseur, G. Haw, C. Croëne, L. Haumesser, A. N. Norris, *Appl. Phys. Lett.* **2013**, 102, 144103.
- [113] R. Zhu, X. N. Liu, G. K. Hu, C. T. Sun, G. L. Huang, *J. Sound Vib.* **2014**, 333, 2759.
- [114] Y. Chen, M. Zheng, X. Liu, Y. Bi, Z. Sun, P. Xiang, J. Yang, G. Hu, *Phys. Rev. B* **2017**, 95, 180104.
- [115] E. Baravelli, M. Ruzzene, *J. Sound Vib.* **2013**, 332, 6562.
- [116] Y. Chen, G. Hu, *Phys. Rev. Appl.* **2019**, 12, 044046.
- [117] J. L. Silverberg, A. A. Evans, L. McLeod, R. C. Hayward, T. Hull, C. D. Santangelo, I. Cohen, *Science* **2014**, 345, 647.
- [118] Y. Tang, G. Lin, S. Yang, Y. K. Yi, R. D. Kamien, J. Yin, *Adv. Mater.* **2017**, 29, 1604262.
- [119] H. Tang, Z. Chen, N. Tang, S. Li, Y. Shen, Y. Peng, X. Zhu, J. Zang, *Adv. Funct. Mater.* **2018**, 28, 1801127.
- [120] H. He, C. Qiu, L. Ye, X. Cai, X. Fan, M. Ke, F. Zhang, Z. Liu, *Nature* **2018**, 560, 61.
- [121] L. Li, A. Haghghi, Y. Yang, *J. Manuf. Process.* **2018**, 33, 150.
- [122] Z. Zeng, Y. Wang, Z. Wang, D. Shan, X. He, *Precis. Eng.* **2012**, 36, 500.
- [123] R. H. Olsson III, I. El-Kady, *Meas. Sci. Technol.* **2009**, 20, 012002.
- [124] Y. Bourquin, R. Wilson, Y. Zhang, J. Reboud, J. M. Cooper, *Adv. Mater.* **2011**, 23, 1458.
- [125] M. Ghasemi Baboly, C. M. Reinke, B. A. Griffin, I. El-Kady, Z. C. Leseman, *Appl. Phys. Lett.* **2018**, 112, 103504.
- [126] S. Krödel, C. Daraio, *Phys. Rev. Appl.* **2016**, 6, 064005.
- [127] D. Qin, Y. Xia, G. M. Whitesides, *Nat. Protoc.* **2010**, 5, 491.
- [128] V. Leroy, A. Bretagne, M. Lanoy, A. Tourin, *AIP Adv.* **2016**, 6, 121604.
- [129] M. Sledzinska, B. Graczykowski, J. Maire, E. Chavez-Angel, C. M. Sotomayor-Torres, F. Alzina, *Adv. Funct. Mater.* **2020**, 30, 1904434.
- [130] Y. Chang, W. Lu, J. Guérolé, L. T. Stephenson, A. Szczepaniak, P. Kontis, A. K. Ackerman, F. F. Dear, I. Mouton, X. Zhong, S. Zhang, D. Dye, C. H. Liebscher, D. Ponge, S. Korte-Kerzel, D. Raabe, B. Gault, *Nat. Commun.* **2019**, 10, 1.
- [131] F. Poratti, S. Barth, R. Sachser, O. V. Dobrovolskiy, A. Seybert, A. S. Frangakis, M. Huth, *ACS Nano* **2019**, 13, 6287.
- [132] D. F. Goettler, M. F. Su, C. M. Reinke, S. Alaie, P. E. Hopkins, R. H. Olsson, I. El-Kady, Z. C. Leseman, *AIP Adv.* **2011**, 1, 042001.

- [133] B. Abad, J. L. Knobloch, T. D. Frazer, J. N. Hernández-Charpak, H. Y. Cheng, A. J. Grede, N. C. Giebink, T. E. Mallouk, P. Mahale, N. N. Nova, A. A. Tomaschke, V. L. Ferguson, V. H. Crespi, V. Gopalan, H. C. Kapteyn, J. V. Badding, M. M. Murnane, *Nano Lett.* **2020**, *20*, 3306.
- [134] J. N. Hernandez-Charpak, K. M. Hoogeboom-Pot, Q. Li, T. D. Frazer, J. L. Knobloch, M. Tripp, S. W. King, E. H. Anderson, W. Chao, M. M. Murnane, H. C. Kapteyn, D. Nardi, *Nano Lett.* **2017**, *17*, 2178.
- [135] J. N. Hernandez-Charpak, J. L. Knobloch, B. Abad Mayor, T. Frazer, H. Kapteyn, M. Murnane, H. Cheng, A. Grede, N. Giebink, T. Mallouk, P. Mahale, W. Chen, Y. Xiong, I. Dabo, V. Crespi, D. Talreja, V. Gopalan, J. Badding, *Health Monitoring of Structural and Biological Systems XII* (Ed: T. Kundu), SPIE, Denver, CO **2018**, p. 69.
- [136] Y. Khan, A. Thielens, S. Muin, J. Ting, C. Baumbauer, A. C. Arias, *Adv. Mater.* **2020**, *32*, 1905279.
- [137] S. Babae, N. Viard, P. Wang, N. X. Fang, K. Bertoldi, *Adv. Mater.* **2016**, *28*, 1631.
- [138] K. H. Lee, K. Yu, A. Xin, Z. Feng, Q. Wang, *Research* **2020**, *2020*, 1.
- [139] R. L. Harne, Y. Song, Q. Dai, *Extrem. Mech. Lett.* **2017**, *12*, 41.
- [140] P. Wang, F. Casadei, S. Shan, J. C. Weaver, K. Bertoldi, *Phys. Rev. Lett.* **2014**, *113*, 014301.
- [141] M. Duranteau, T. Valier-Brasier, J.-M. Conoir, R. Wunenburger, *J. Acoust. Soc. Am.* **2016**, *139*, 3341.
- [142] T. Zhang, R. A. Sanguramath, S. Israel, M. S. Silverstein, *Macromolecules* **2019**, *52*, 5445.
- [143] K. Zimny, A. Merlin, A. Ba, C. Aristégui, T. Brunet, O. Mondain-Monval, *Langmuir* **2015**, *31*, 3215.
- [144] Y. Jin, R. Kumar, O. Poncelet, O. Mondain-Monval, T. Brunet, *Nat. Commun.* **2019**, *10*, 1.
- [145] L. Lukyanova, L. Séon, A. Aradian, O. Mondain-Monval, J. Leng, R. Wunenburger, *J. Appl. Polym. Sci.* **2013**, *128*, 3512.
- [146] Z. Liu, *Science* **2000**, *289*, 1734.
- [147] Z. Liu, C. T. Chan, P. Sheng, *Phys. Rev. B* **2005**, *71*, 014103.
- [148] B.-I. Popa, S. A. Cummer, *Nat. Commun.* **2014**, *5*, 3398.
- [149] P. H. Otsuka, S. Mezil, O. Matsuda, M. Tomoda, A. A. Maznev, T. Gan, N. Fang, N. Boechler, V. E. Gusev, O. B. Wright, *New J. Phys.* **2018**, *20*, 013026.
- [150] P. Celli, S. Gonella, *Appl. Phys. Lett.* **2015**, *107*, 081901.
- [151] N. Sui, X. Yan, T.-Y. Huang, J. Xu, F.-G. Yuan, Y. Jing, *Appl. Phys. Lett.* **2015**, *106*, 171905.
- [152] F. Casadei, T. Delpero, A. Bergamini, P. Ermanni, M. Ruzzene, *J. Appl. Phys.* **2012**, *112*, 064902.
- [153] A. Marzo, M. Caleap, B. W. Drinkwater, *Phys. Rev. Lett.* **2018**, *120*, 044301.
- [154] L. Cox, A. Croxford, B. W. Drinkwater, A. Marzo, *Appl. Phys. Lett.* **2018**, *113*, 054101.
- [155] S. Inoue, S. Mogami, T. Ichiyama, A. Noda, Y. Makino, H. Shinoda, *J. Acoust. Soc. Am.* **2019**, *145*, 328.
- [156] J. K. Eliason, A. Vega-Flick, M. Hiraiwa, A. Khanolkar, T. Gan, N. Boechler, N. Fang, K. A. Nelson, A. A. Maznev, *Appl. Phys. Lett.* **2016**, *108*, 061907.
- [157] A. Khanolkar, S. Wallen, M. Abi Ghanem, J. Jenks, N. Vogel, N. Boechler, *Appl. Phys. Lett.* **2015**, *107*, 071903.
- [158] G. Ji, Y. Fang, J. Zhou, X. Huang, *J. Appl. Phys.* **2019**, *125*, 215110.
- [159] S. Yves, F. Lemoult, M. Fink, G. Lerosey, *Sci. Rep.* **2017**, *7*, 15359.
- [160] H. Esfahlani, H. Lissek, J. R. Mosig, *Phys. Rev. B* **2017**, *95*, 024312.
- [161] M. Yang, S. Chen, C. Fu, P. Sheng, *Mater. Horizons* **2017**, *4*, 673.
- [162] F. Lucklum, M. J. Vellekoop, *Procedia Eng.* **2015**, *120*, 1095.
- [163] F. G. Woodhouse, J. Dunkel, *Nat. Commun.* **2017**, *8*, 1.
- [164] L. Q. Tao, H. Tian, Y. Liu, Z. Y. Ju, Y. Pang, Y. Q. Chen, D. Y. Wang, X. G. Tian, J. C. Yan, N. Q. Deng, Y. Yang, T. L. Ren, *Nat. Commun.* **2017**, *8*, 1.
- [165] X. Xia, A. Afshar, H. Yang, C. M. Portela, D. M. Kochmann, C. V. Di Leo, J. R. Greer, *Nature* **2019**, *573*, 205.
- [166] J. Bauer, L. R. Meza, T. A. Schaedler, R. Schwaiger, X. Zheng, L. Valdevit, *Adv. Mater.* **2017**, *29*, 1701850.
- [167] T. Frenzel, M. Kadic, M. Wegener, *Science* **2017**, *358*, 1072.
- [168] Y. Zhang, F. Zhang, Z. Yan, Q. Ma, X. Li, Y. Huang, J. A. Rogers, *Nat. Rev. Mater.* **2017**, *2*, 17019.
- [169] H. N. Chan, Y. Shu, Q. Tian, Y. Chen, Y. Chen, H. Wu, *Mater. Horizons* **2016**, *3*, 309.
- [170] Y. Gao, J. Song, S. Li, C. Elowsky, Y. Zhou, S. Ducharme, Y. M. Chen, Q. Zhou, L. Tan, *Nat. Commun.* **2016**, *7*, 12316.
- [171] N. Kleger, M. Cihova, K. Masania, A. R. Studart, J. F. Löffler, *Adv. Mater.* **2019**, *31*, 1903783.



**Christabel Choi** is a Ph.D. student in metamaterials in the Department of Computer Science at University College London, UK. Under the supervision of Professor Sriram Subramanian, her research focus is on the development and fabrication of actively reconfigurable acoustic metamaterials. At the University of Sussex, Falmer, UK, she received her B.Eng. in Electrical and Electronic Engineering in 2018, before joining the Interact Lab from 2019 to 2020.



**Shubhi Bansal** is a postdoctoral research fellow at University College London, UK. She received her Ph.D. along with M.Sc. (Engineering) in Nano Science and Engineering from Indian Institute of Science, India, in 2018. She received her B.Tech. in Engineering Physics (with a Major in Electronics and Minor in Material Science and Technology) from Delhi Technological University, India, in 2013. She was a research associate at Indian Institute of Science, India, from 2018 to 2019. She subsequently worked as a postdoctoral research fellow with Interact Lab at the University of Sussex, Falmer, UK, from 2019 to 2020.





**Niko Münzenrieder** is an associate professor for Physics of Matter at the Free University of Bozen-Bolzano, Italy, where he is working on thin-film technology as well as flexible and wearable electronics. He received a diploma in physics from the Technical University of Munich, Germany, in 2008, and a Ph.D. in electrical engineering from the Swiss Federal Institute of Technology (ETH) Zürich, Switzerland, in 2013, where he also worked as a postdoctoral research fellow in 2014. From 2015 to 2019 he was a lecturer, later senior lecturer, with the Sensor Technology Research Centre at the University of Sussex, Brighton, UK.



**Sriram Subramanian** is a Royal Academy of Engineering Chair in Emerging Technologies at University College London (UK), where he leads a research group on designing interactive applications using acoustic metamaterials and phased arrays. Before joining UCL he was a professor of human–computer interaction at the University of Sussex (2015–2020) and University of Bristol (2007–2015).